AD-A116 399 TEXAS UNIV AT AUSTIN APPLIED RESEARCH LABS F/G 20/1
ACOUSTIC REFLECTION FROM ANISOTROPIC SEDIMENTS.(U)
JUN 82 D W OAKLEY N00014-80-C-0490
UNCLASSIFIED ARL-TR-82-28 NL

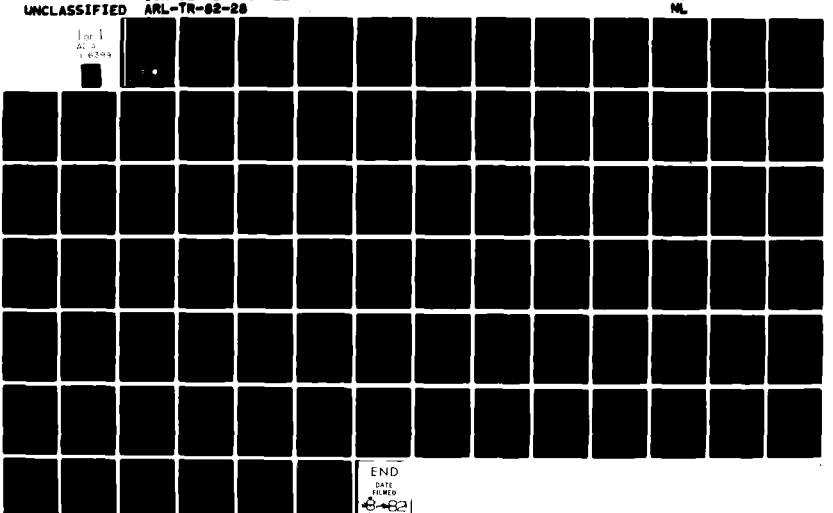

END
DATE FILMED
DTIC

(12)

AD A116399

ARL-TR-82-28

Copy No. 27

ACOUSTIC REFLECTION FROM ANISOTROPIC SEDIMENTS

David W. Oakley

APPLIED RESEARCH LABORATORIES
THE UNIVERSITY OF TEXAS AT AUSTIN
POST OFFICE BOX 8029, AUSTIN, TEXAS 78712-8029

1 June 1982

Technical Report

Prepared for:

OFFICE OF NAVAL RESEARCH
DEPARTMENT OF THE NAVY
ARLINGTON, VA 22217

UNCLASSIFIED

SECURITY CLASSIFICATION OF THIS PAGE *(When Data Entered)*

REPORT DOCUMENTATION PAGE		READ INSTRUCTIONS BEFORE COMPLETING FORM
1. REPORT NUMBER	2. GOVT ACCESSION NO. AD-A116 399	3. RECIPIENT'S CATALOG NUMBER
4. TITLE *(and Subtitle)* ACOUSTIC REFLECTION FROM ANISOTROPIC SEDIMENTS		5. TYPE OF REPORT & PERIOD COVERED technical report
		6. PERFORMING ORG. REPORT NUMBER ARL-TR-82-28
7. AUTHOR(s) David W. Oakley		8. CONTRACT OR GRANT NUMBER(s) N00014-80-C-0490
9. PERFORMING ORGANIZATION NAME AND ADDRESS Applied Research Laboratories The University of Texas at Austin Austin, Texas 78712-8029		10. PROGRAM ELEMENT, PROJECT, TASK AREA & WORK UNIT NUMBERS Item 0015
11. CONTROLLING OFFICE NAME AND ADDRESS Office of Naval Research Department of the Navy Arlington, VA 22217		12. REPORT DATE 1 June 1982
		13. NUMBER OF PAGES
14. MONITORING AGENCY NAME & ADDRESS*(if different from Controlling Office)*		15. SECURITY CLASS. *(of this report)* UNCLASSIFIED
		15a. DECLASSIFICATION/DOWNGRADING SCHEDULE

16. DISTRIBUTION STATEMENT *(of this Report)*

Approved for public release; distribution unlimited.

17. DISTRIBUTION STATEMENT *(of the abstract entered in Block 20, if different from Report)*

18. SUPPLEMENTARY NOTES

19. KEY WORDS *(Continue on reverse side if necessary and identify by block number)*

20. ABSTRACT *(Continue on reverse side if necessary and identify by block number)*

Measurements of an excess of horizontal to vertical velocity (averaging 10% for shales) have been made in marine sediments and in sedimentary rocks. In this paper, the proposed causes of such anisotropies are reviewed, and the reflection coefficient for incidence from water onto a solid sea floor is derived for plane wave solutions of the anisotropic wave equations. The possibility of backward traveling fronts of pressure amplitude at low grazing angles is noted. A propagation matrix formation is established to generalize the reflection coefficient for the case of multiple layers. Bottom loss

DD FORM 1 JAN 73 1473 EDITION OF 1 NOV 65 IS OBSOLETE

UNCLASSIFIED

SECURITY CLASSIFICATION OF THIS PAGE *(When Data Entered)*

20. (Cont'd)

calculations are made which suggest that anisotropy can increase the reflectivity of the ocean floor.

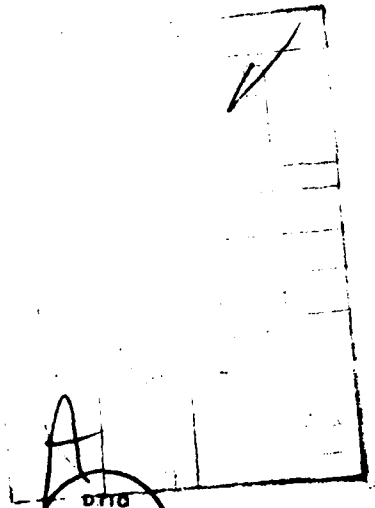

TABLE OF CONTENTS

LIST OF TABLES

LIST OF FIGURES

CHAPTER I

INTRODUCTION

Customary studies of acoustic bottom interation model the sea floor as a series of flat, isotropic layers underlaid by a flat, semi-infinite homogeneous isotropic substrate. However, it has always been recognized that this model represents an extreme idealization of the actual bottom environment.

The assumption of isotropy of sediments has always been known to be incorrect on a microscopic scale. The mineral grains composing the various sediments are inherently anisotropic. Acousticians have assumed that because these anisotropic grains are randomly distributed, the sediment therefore presents overall isotropy.

Unfortunately, experimental evidence does not bear out this assumption. Petroleum geophysicists have reported velocity anisotropies from their well log data for many years and the work of the Deep Sea Drilling Project (DSDP) has confirmed that velocity anisotropies do, indeed, exist in marine sediments.

It is the purpose of this paper, therefore, to examine the causes of velocity anisotropies in sediments and the properties of those sediments, and to develop the mathematical theory of reflection from such sediments. The particular mathematical framework which has been chosen is that for transversely isotropic layers, that is, layers which have a single

unique axis, and rotational symmetry about that axis. Propagation in such a medium will be examined, and a parameterized version of a reflection coefficient model developed. The theory utilized in the work is based on that of Stoneley. His derivation of the equation of motion is followed and used as a basis for our derivation of the reflection coefficient.

Chapter II of this work is a discussion of observed anisotropies in marine sediments and the mechanisms considered responsible for such anisotropies. The theoretical form of the reflection coefficient is derived in Chapter III, and in Chapter IV the results of numerical calculations in the formulation are compared with those of standard isotropic theory.

CHAPTER II

OCCURRENCE AND CAUSES OF VELOCITY ANISOTROPY

The most commonly noticed anisotropy in marine sediments is an excess of the parallel shear and compressional velocities over the velocities normal to the plane of bedding. Hamilton (1970) concludes from data obtained by LeRoy (1950) and Uhrig and Van Melle (1955) that shale exhibits an average anisotropy of horizontal over vertical velocities of about 10%, though the excess may run as high as 40%.

Milholland, Manghnani, Schlanger, and Sutton (1980) state a measure for this anisotropy,

$$A = \frac{\overline{V}_h - \overline{V}_v}{\overline{V}} \quad ,$$

where subscripts h and v refer to the directions parallel and normal, respectively, to the plane of bedding, V refers to velocity, and superscripted bars refer to averages. This same formula produces shear and compressional anisotropies, A_p and A_s, but it must be remembered that the propagation of a shear wave along a given direction is also dependent upon its polarization. Six measurements must therefore be taken to characterize V for shear waves, measurements along each axis being taken with polarizations both parallel and perpendicular to the plane of bedding. It is this definition of anisotropy which is used throughout this paper.

Milholland, Manghnani, Schlanger, and Sutton (1980) also define a second parameter,

$$A_{so} = \frac{\bar{V}_s^{hh} - \bar{V}_s^{hv}}{\bar{V}_s} \quad ,$$

which measures the anisotropy of horizontally propagating waves (first superscript) with polarization (second superscript) parallel and normal to the plane of bedding. This quantity is of more value than A_s from a theoretical viewpoint, as it can be related to the elastic constants of the sediment.

In oozes and chalks, Manghnani, Schlanger, and Milholland (1980) report variations in compressional anisotropy from -4% to 8%, and variations in shear anisotropy from -8% to 6%. In carbonate limestones, siliceous limestones, and chert below 1020 m they have determined the compressional anisotropy to be 8% ±4%, and the shear anisotropy to be 6% ±4%.

In a later report from this same group of geophysicists (Milholland et al., 1980), data from the DSDP is used to obtain a more detailed picture of the velocity anisotropies of marine sediments. These results are reproduced in Table I.

It is to be noted from Table I that carbonate limestones, siliceous limestones, and cherts have similar velocity anisotropies. This similarity would seem to imply that silica content does not contribute significantly to velocity anisotropy. On the other hand, clay enrichment of calcareous sediments increases velocity anisotropies, whereas non-calcareous clays show a much smaller degree of anisotropy. Velocity

TABLE I

REPRESENTATIVE VELOCITY ANISOTROPIES

FROM DSDP DATA

Sites 288, 299	A_p (%)	A_s (%)	A_{so} (%)
Carbonate Ooze	2.0		
Carbonate Chalk	2.9 (3.3)	0.5 (4.7)	2.7 (4.2)
Carbonate Limestone	8.0 (4.7)	6.2 (4.9)	7.9 (4.7)
Siliceous Limestone	8.6 (3.7)	5.6 (3.4)	5.9 (4.0)
Chert	8.3 (2.3)	6.3 (2.0)	6.2 (3.7)
Basalt	2.5 (1.0)		

Site 210	A_p (%)	A_s (%)	A_{so} (%)
Clay-bearing Ooze & Chalk	6.2 (1.4)	6.63 (3.7)	9.6 (4.5)
Clay-rich Chalk	6.8 (2.6)	14.2 (5.9)	9.2 (6.4)
Calcic-rich Chalk	8.1 (1.2)	17.4 (5.0	23.0 (5.6)
Non-calcareous Clay	3.3 (1.2)	-0.4 (2.4)	12.2 (6.7)

The numbers in parentheses represent the standard deviation for the corresponding sediment type.

anisotropies in clay-bearing to clay-rich oozes and chalk are approximately twice as large as in calcareous oozes and chalks. Furthermore, shear anisotropies and shear orientation anisotropies tend to be greater than compressional anisotropies for clay-bearing sediments, whereas the compressional anisotropy is greater than the shear and shear orientation velocities in more calcareous sediments.

Carlson and Christensen (1979) show that velocity anisotropies are well developed at less than 0.4 km into the sediment and that anisotropy increases markedly with depth (depth below sea level is not meant here, but depth of overburden). Concurrent with this depth dependent increase in anisotropies are related increases in anisotropy with increasing density, and with increasing mean velocity.

Several different approaches have been taken toward finding a physical mechanism which would explain the existence of transversely isotropic sediments. Hamilton (1970) considered overburden pressure acting upon clay as a cause of such a system. Since clay has a flocculated (collapsed house of cards) structure, sufficient pressure should lead to an ordering of the clay structure in which the platelets would assume positions parallel to the plane of bedding. Hamilton realized, however, that such a purely mechanical action upon clay could not produce the observed anisotropies at depths shallower than 400-600 m, although a measurable anisotropy would be produced at these depths. This explanation of sediment velocity anisotropy has not proved very useful, however, as it is geared to explain pure silt and clay sediments, which actually show much smaller degrees of anisotropy than other sediments; a non-calcareous clay from DSDP Site 210 shows a compressional anisotropy of

3.3% and a shear anisotropy essentially zero, while a clay enriched carbonate ooze and chalk from the same site shows a compressional anisotrophy of 6.2% and a shear anisotrophy of 6.63%.

Carlson and Christensen (1979) proposed mechanisms for explaining the larger velocity anisotropies in calcareous sediments. They discounted the first mechanism, the alignment of cracks and pores in the bedding plane, because it is known that pores and cracks close under increasing pressure; this would cause the vertical velocity to increase more rapidly than horizontal velocities with depth, an equality (isotropy) eventually being reached. Since anisotropy increases with depth, this mechanism cannot be the driving mechanism for transverse isotropy.

The second mechanism examined by Carlson and Christensen (1979) seem to be the most adequate in explaining the observed phenomena. If the calcite crystals in calcareous sediments have a preferred orientation, anisotropies of the preferred type (i.e., transverse isotropy) would result. Dandekar (1968) determined that calcite crystals exhibit a velocity of 5.61 km/sec parallel to their c-axes, and a velocity of 7.35 km/sec normal to their c-axes (the c-axis is that direction along which a ray of light is not doubly refracted). Therefore, if it could be ascertained that calcite grains align their c-axes normal to the plane of bedding, the observed anisotropies would be accounted for. Manghnani, Schlanger, and Milholland (1980) reported that preliminary X-ray petrofabric data for carbonate sediment core samples from DSDP Site 289 show such a preferential orientation of the calcite c-axes.

Carlson and Christensen (1979) and Manghnani, Schlanger, and Milholland (1980) pointed out that calcareous deep sea sediments consist

almost exclusively of biogenic detritus. Prominent among the various detritus in calcareous sediments are various members of the genus Coccolithus and the genus Cyclococcolithina, and discoasters. In these organisms, calcite crystals contained in the disc shaped skeletons are aligned with their c-axes normal to the long dimensions of the microfossils. Though these disc-like forms are randomly oriented in oozes, increasing compaction leads to their alignment parallel with the plane of bedding, leaving the calcite crystal c-axes normal to the plane of bedding.

This pressure induced alignment of c-axes is only the beginning of the ordering of carbonate sediments, however. The diagenetic model of Schlanger and Douglas (1974) posits that the major change in the transformation of carbonate ooze to chalk to limestone is the solution and reprecipitation of the carbonate as cement. Elimination of crystal defects such as the presence of strontium, dissolution of small crystals, and the growth of larger crystals reduce the free energy of the system. Furthermore, Carlson and Christensen (1979), reporting from Bain (1940) and Bukry (1971), conclude that calcite crystals with faces nearly perpendicular to the c-axes are more resistant to dissolution than those with faces nearly parallel. Hence, those microforms most resistant to solution are those which have their c-axes normal to their long dimension. In other words, the process of solution and recrystallization in calcite operates in such a manner that most calcite c-axes are normal to the plane of bedding, thus producing a larger velocity of propagation parallel to the bedding plane than normal to it.

Milholland, Manghnani, Schlanger, and Sutton (1980) believe that the role of clay enrichment in increasing velocity anisotropy is

best explained by the mechanism proposed in Weyl (1952). According to this model, clay particles, being much smaller and more plastic than the calcite crystals, coat calcite grains with an ooze, reducing the point-to-point contacts of crystals, and increasing the total reactive surface, thus catalyzing the solution and recrystallization of calcite at a rate more rapid than normal.

In summary, many measurements of anisotropy establish values of 0-15% with 10% being typical. Many mechanisms have been proposed to account for such anisotropies, including pore and crack alignment, overburden pressure, and the alignment of calcite crystals. We conclude that, while overburden pressure plays a minor role in determining velocity anisotropies, the principal cause of such anisotropies is the presence of calcite crystals aligned with their c-axes normal to the plane of bedding. The mechanism that best explains this is the deposition of certain biogenic detritus and their subsequent dissolution and recrystallization with the proper alignment. The existence of such alignments has been confirmed experimentally.

CHAPTER III

THEORY OF REFLECTION FROM TRANSVERSELY ANISOTROPIC SOLIDS

From the data and geological models available, it is reasonable to model an anisotropic sediment as a transversely isotropic solid, that is, as a body containing a single unique axis, all rotations about the axis being equivalent. This axis will be taken to be the z-axis, perpendicular to the plane of bedding.

A. Independent Elastic Parameters for Transverse Isotropy

The first problem which arises from a departure from isotropy is an increase in the number of independent elastic parameters of the system. While an isotropic system has but two independent elastic parameters, a transversely anisotropic system has five. In obtaining these constants, we shall follow the development of Love (1944), in a somewhat more modern notation. If one begins from the stress-strain relation, Hooke's Law,

$$S_{ij} = C_{ijkl} e_{kl} \quad ,$$

there are a total of 81 possible elastic parameters. Here S_{ij}, e_{kl}, and C_{ijkl} are the components of the stress, strain, and elastic tensors, respectively, and repeated indices are summed over. However, a set of equivalences,

$$C_{ijkl} = C_{klij} = C_{jikl} = C_{ijlk} \quad ,$$

reduces the number of independent elastic parameters to 21 in the case of complete anisotropy. The set of equivalences springs, respectively, from the conditions that a thermodynamic internal energy exists, that the stress S_{ij} is symmetric, and that the strain e_{kl} is symmetric under interchange of index.

To simplify the notation, the elements of these tensors are identified with the components of a symmetric 6 x 6 matrix. The following associations of subscripts are made: xx=1, yy=2, zz=3, yz=4, zx=5, xy=6. Thus, the stress-strain relation may be rewritten using this notation as

$$S_I = C_{IJ}e_J \quad .$$

To further reduce the number of independent elastic parameters, let us utilize the strain-energy function, defined by the relation

$$S_I = \frac{\partial W}{\partial e_I} \quad .$$

As discussed in Love (1944) and Aki and Richards (1980) the actual quantity chosen for W may be either the free energy or the internal energy, depending upon whether conditions are isothermal or adiabatic. It is standard in most texts to choose adiabatic conditions, since at

wavelengths greater than a few millimeters the thermal diffusion coefficient in sediments is much longer than the period of elastic waves. Combining Hooke's Law with the defining relation for W, one obtains the result:

$$2W = C_{IJ}e_I e_J \quad .$$

Written in its entirety, this equation is:

$$\begin{aligned} 2W = {} & C_{11}e_1^2 + 2C_{12}e_1e_2 + 2C_{13}e_1c_3 + 2C_{14}e_1e_4 \\ & + 2C_{15}e_1e_5 + 2C_{16}e_1e_6 + C_{22}e_2^2 + 2C_{23}e_2e_3 \\ & + 2C_{24}e_2e_4 + 2C_{25}e_2e_5 + 2C_{26}e_2e_6 + C_{33}e_3^2 \\ & + 2C_{34}e_3e_4 + 2C_{35}e_3e_5 + 2C_{36}e_3e_6 + C_{44}e_4^2 \\ & + 2C_{45}e_4e_5 + 2C_{46}e_4e_6 + C_{55}e_5^2 \\ & + 2C_{56}e_5e_6 + C_{66}e_6^2 \quad . \end{aligned}$$

We now demand, for transverse anisotropy, that this quantity be invariant under a rotation about the z-axis. Under a rotation of angle θ about the z-axis, the strains take the form

$$e_{1'} = e_1\cos^2\theta + e_2\sin^2\theta + e_6\sin\theta\cos\theta \quad ,$$

$$e_{2'} = e_1\sin^2\theta + e_2\cos^2\theta - e_6\sin\theta\cos\theta \quad ,$$

$$e_{3'} = e_3 \quad ,$$

$$e_{4'} = e_4\cos\theta - e_5\sin\theta \quad ,$$

$$e_{5'} = e_4\sin\theta + e_5\cos\theta \quad ,$$

$$e_{6'} = -2e_1\sin\theta\cos\theta + 2e_2\sin\theta\cos\theta + e_6(\cos^2\theta - \sin^2\theta) \quad ,$$

where primes refer to the values of the strains in the rotated system.

If these substitutions are made into the strain-energy function and coefficients of corresponding strain products are equated, a set of 21 equations is obtained. Fortunately, this set of equations can be partitioned into smaller subsets, corresponding to a partition of the set of elastic parameters.

Consider the subset obtained by equating the coefficients of the products e_1e_1, e_2e_2, e_1e_2, e_1e_6, e_2e_6, and e_6e_6, respectively:

$$C_{11} = C_{11}\cos^4\theta + 2C_{12}\cos^2\theta\sin^2\theta - 4C_{16}\sin\theta\cos^3\theta$$

$$+ C_{22}\sin^4\theta - 4C_{26}\sin^3\theta\cos\theta + 4C_{66}\sin^2\theta\cos\theta \quad ,$$

$$C_{22} = C_{11}\sin^4\theta + 2C_{12}\cos^2\theta\sin^2\theta + 4C_{16}\sin^3\theta\cos\theta$$

$$+ C_{22}\cos^4\theta + 4C_{26}\sin\theta\cos^3\theta + 4C_{66}\sin^2\theta\cos^2\theta \quad ,$$

$$C_{12} = C_{11}\cos^2\theta\sin^2\theta + C_{12}(\cos^4\theta+\sin^4\theta) + 2C_{16}\sin\theta\cos\theta(\cos^2\theta-\sin^2\theta)$$

$$+ C_{22}\sin^2\theta\cos^2\theta - 2C_{26}\sin\theta\cos\theta(\cos^2\theta-\sin^2\theta) - 4C_{66}\sin^2\theta\cos^2\theta \quad ,$$

$$C_{16} = C_{11}\sin\theta\cos^3\theta + C_{12}\sin\theta\cos\theta(\sin^2\theta-\cos^2\theta) + C_{16}(\cos^4\theta-3\cos^2\theta\sin^2\theta)$$

$$- C_{22}\sin^3\theta\cos\theta - C_{26}(\sin^4\theta-3\cos^2\theta\sin^2\theta) - 2C_{66}\sin\theta\cos\theta(\cos^2\theta-\sin^2\theta) \quad ,$$

$$C_{26} = C_{11}\sin^3\theta\cos\theta + C_{12}\sin\theta\cos\theta(\cos^2\theta-\sin^2\theta) - C_{16}(\sin^4\theta-3\cos^2\theta\sin^2\theta)$$

$$- C_{22}\sin\theta\cos^3\theta + C_{26}(\cos^4\theta-3\cos^2\theta\sin^2\theta) + 2C_{66}\sin\theta\cos\theta(\cos^2\theta-\sin^2\theta) \quad ,$$

$$C_{66} = C_{11}\sin^2\theta\cos^2\theta - 2C_{12}\sin^2\theta\cos^2\theta + 4C_{16}\sin\theta\cos\theta(\cos^2\theta-\sin^2\theta)$$

$$+ C_{22}\sin^2\theta\cos^2\theta - 4C_{26}\sin\theta\cos\theta(\cos^2\theta-\sin^2\theta) + C_{66}(\cos^2\theta-\sin^2\theta)^2 \quad .$$

Adding the fifth and sixth equations, then subtracting the second equation from the first, and removing a factor of $\sin\theta$ from both results yields

$$0 = (C_{11}-C_{22})\cos\theta - 2(C_{16}+C_{26})\sin\theta \quad ,$$

$$0 = (C_{11}-C_{22})\cos\theta + 2(C_{16}+C_{26})\sin\theta \quad .$$

Solving for $C_{11}-C_{22}$ and $C_{16}+C_{26}$ yields

$$C_{11} = C_{22} \quad ,$$

$$C_{26} = C_{16} \quad .$$

Substituting these results into the third and sixth equations and combining like terms, one obtains

$$0 = 2C_{11}\cos^2\theta\sin^2\theta - 2C_{12}\sin^2\theta\cos^2\theta$$

$$+ 4C_{16}\cos\theta\sin\theta(\cos^2\theta-\sin^2\theta) - 4C_{66}\sin^2\theta\cos^2\theta \quad ,$$

$$0 = 2C_{11}\cos^2\theta\sin^2\theta - 2C_{12}\sin^2\theta\cos^2\theta$$

$$+ 8C_{16}\cos\theta\sin\theta(\cos^2\theta-\sin^2\theta) - 4C_{66}\sin^2\theta\cos^2\theta \quad .$$

On substituting these two equations, it is obvious that

$$C_{16} = C_{26} = 0 \quad .$$

Making this substitution and removing a factor of $2\cos^2\theta\sin^2\theta$, one obtains

$$C_{66} = 1/2(C_{11}-C_{12}) \quad .$$

Let us next consider the second set of equations, obtained by equating the coefficients by e_1e_3, e_2e_3, and e_3e_6, respectively,

$$C_{13} = C_{13}\cos^2\theta + C_{23}\sin^2\theta - 2C_{36}\sin\theta\cos\theta \quad ,$$

$$C_{23} = C_{13}\sin^2\theta + C_{23}\cos^2\theta + 2C_{36}\sin\theta\cos\theta \quad ,$$

$$C_{36} = C_{13}\sin\theta\cos\theta - C_{23}\sin\theta\cos\theta + C_{36}(\cos^2\theta-\sin^2\theta) \quad .$$

Simplifying the first two equations yields

$$0 = (C_{23}-C_{13})\sin^2\theta - 2C_{36}\sin\theta\cos\theta \quad ,$$

$$0 = (C_{13}-C_{23})\cos^2\theta - 2C_{36}\sin\theta\cos\theta \quad ,$$

which are correct at $\sin\theta=0$ or $\cos\theta=0$ only if

$$C_{13} = C_{23} \quad ,$$

from which it follows

$$C_{36} = 0 \quad .$$

The third set of equations, arising from equating coefficients of e_4e_4, e_4e_5, and e_5e_5, is

$$C_{44} = C_{44}\cos^2\theta + 2C_{45}\cos\theta\sin\theta + C_{55}\sin^2\theta \quad ,$$

$$C_{45} = C_{44}\cos\theta\sin\theta + C_{45}(\cos^2\theta - \sin^2\theta) + C_{55}\sin\theta\cos\theta \quad ,$$

$$C_{55} = C_{44}\sin^2\theta - 2C_{45}\sin\theta\cos\theta + C_{55}\cos^2\theta \quad .$$

Simplifying the first two equations yields

$$0 = -C_{44}\sin\theta + 2C_{45}\cos\theta + C_{55}\sin\theta \quad ,$$

$$0 = -C_{44}\cos\theta - 2C_{45}\sin\theta + C_{55}\cos\theta \quad ,$$

which has a solution consistent with the third equation,

$$C_{44} = C_{55} \quad ,$$

and

$$C_{45} = 0 \quad .$$

The fourth set of equations, obtained from equating coefficients by e_3e_4 and e_3e_5, is

$$C_{34} = C_{34}\cos\theta + C_{35}\sin\theta \quad ,$$

$$C_{35} = -C_{34}\sin\theta + C_{35}\cos\theta \quad .$$

Consistency at $\cos\theta=0$ demands

$$C_{34} = C_{35} = 0 \quad .$$

The fifth subset of equations yields no new information. The final subset, obtained by equating coefficients by e_1e_4, e_1e_5, e_2e_4, e_2e_5, e_4e_6, and e_5e_6, yields:

$$C_{14} = C_{14}\cos^3\theta + C_{15}\sin\theta\cos^2\theta + C_{24}\sin^2\theta\cos\theta$$
$$+ C_{25}\sin^3\theta - 2C_{46}\sin\theta\cos^2\theta - 2C_{56}\sin^3\theta\cos\theta \quad ,$$

$$C_{15} = -C_{14}\sin\theta\cos^2\theta + C_{15}\cos^3\theta - C_{24}\sin^3\theta$$
$$+ C_{25}\sin^2\theta\cos\theta + 2C_{46}\sin^2\theta\cos\theta - 2C_{56}\sin\theta\cos^2\theta \quad ,$$

$$C_{24} = C_{14}\sin^2\theta\cos\theta + C_{15}\sin^3\theta + C_{24}\cos^3\theta$$
$$+ C_{25}\sin\theta\cos^2\theta + 2C_{46}\sin\theta\cos^2\theta + 2C_{56}\sin^2\theta\cos\theta \quad ,$$

$$C_{25} = -C_{14}\sin^3\theta + C_{15}\sin^2\theta\cos\theta - C_{24}\sin\theta\cos^2\theta$$
$$+ C_{25}\cos^3\theta - 2C_{46}\sin^2\theta\cos\theta + 2C_{56}\sin\theta\cos^2\theta \quad ,$$

$$C_{46} = C_{14}\sin\theta\cos^2\theta + C_{15}\sin^2\theta\cos\theta - C_{24}\sin\theta\cos^2\theta$$

$$- C_{25}\sin^2\theta\cos\theta + C_{46}\cos\theta(\cos^2\theta-\sin^2\theta) + C_{56}\sin\theta(\cos^2\theta-\sin^2\theta) \quad ,$$

$$C_{56} = C_{14}\sin^2\theta\cos\theta + C_{15}\sin\theta\cos^2\theta + C_{24}\sin^2\theta\cos\theta$$

$$- C_{25}\sin\theta\cos^2\theta - C_{46}\sin\theta(\cos^2\theta-\sin^2\theta) + C_{56}\cos\theta(\cos^2\theta-\sin^2\theta) \quad .$$

At $\cos\theta=0$, the first, fourth, fifth, and sixth equations become

$$C_{14} = C_{25} \quad ,$$

$$C_{25} = -C_{14} \quad ,$$

$$C_{46} = -C_{56} \quad ,$$

$$C_{56} = C_{46} \quad ,$$

which can be consistent only if

$$C_{14} = C_{25} = C_{56} = C_{46} = 0 \quad .$$

At $\sin\theta=\cos\theta=1/\sqrt{2}$, the first and fourth equations become

$$0 = C_{15} - C_{24} \quad ,$$

$$0 = C_{15} + C_{24} \quad ,$$

which can be consistent only if

$$C_{15} = C_{24} = 0 \quad .$$

Combining all these results, the strain-energy function may, for transversely isotropic media, be written in terms of only five parameters (C_{11}, C_{12}, C_{33}, C_{13}, C_{44}), as

$$2W = C_{11}(e_1^2+e_2^2) + C_{33}e_3^2 + 2C_{13}(e_1+e_2)e_3$$

$$+ 2C_{12}e_1e_2 + C_{44}(e_4^2+e_5^2) + C_{66}e_6^2 \quad ,$$

where $C_{66} = 1/2(C_{11}-C_{12})$.

B. Equations of Motion for Transversely Isotropic Media

Reverting to our initial notation, the equation of motion may be obtained from the potential energy via the stresses:

$$\rho \frac{\partial^2 u_i}{\partial t^2} = \frac{\partial S_{ij}}{\partial x^j} \quad ,$$

where $S_{ij} = \partial w/\partial e_{ij}$, ρ is the density, the quantities u_i are the components of displacement, and t is the time. Substituting

$$e_{ii} = \frac{\partial u_i}{\partial x^i}$$

and

$$e_{ij} = \frac{\partial u_i}{\partial x^j} + \frac{\partial u_j}{\partial x^i}$$

into the equations of motion, one obtains the set of equations

$$\rho \frac{\partial^2 u}{\partial t^2} = \frac{\partial}{\partial x}\left\{C_{11}\frac{\partial u}{\partial x} + C_{12}\frac{\partial v}{\partial y} + C_{13}\frac{\partial w}{\partial z}\right\} + \frac{\partial}{\partial y}\left\{C_{66}\left(\frac{\partial u}{\partial y} + \frac{\partial v}{\partial x}\right)\right\}$$

$$+ \frac{\partial}{\partial z}\left\{C_{44}\left(\frac{\partial u}{\partial z} + \frac{\partial w}{\partial x}\right)\right\} \quad ,$$

$$\rho \frac{\partial^2 v}{\partial t^2} = \frac{\partial}{\partial x}\left\{C_{66}\left(\frac{\partial u}{\partial y} + \frac{\partial v}{\partial x}\right)\right\} + \frac{\partial}{\partial y}\left\{C_{12}\frac{\partial u}{\partial x} + C_{11}\frac{\partial v}{\partial y} + C_{13}\frac{\partial w}{\partial z}\right\}$$

$$+ \frac{\partial}{\partial z}\left\{C_{44}\left(\frac{\partial v}{\partial z} + \frac{\partial w}{\partial y}\right)\right\} \quad ,$$

$$\rho \frac{\partial^2 w}{\partial t^2} = \frac{\partial}{\partial x}\left\{C_{44}\left(\frac{\partial u}{\partial z} + \frac{\partial w}{\partial x}\right)\right\} + \frac{\partial}{\partial y}\left\{C_{44}\left(\frac{\partial v}{\partial z} + \frac{\partial w}{\partial y}\right)\right\}$$

$$+ \frac{\partial}{\partial z}\left\{C_{13}\left(\frac{\partial u}{\partial x} + \frac{\partial v}{\partial y}\right) + C_{33}\frac{\partial w}{\partial z}\right\} \quad ,$$

where u, v, w have been substituted for the components of the displacement vectors u_x, u_y, u_z, respectively.

In order to attach a bit more physical intuition to these equations, let us examine waves whose propagation and polarization are both along the coordinate axes.

For an x-propagating (v=w=0) or a y-propagating (u=w=0) compressional wave, the equations of motion reduce to

$$\rho \frac{\partial^2 u}{\partial t^2} = C_{11} \frac{\partial^2 u}{\partial x^2}$$

or

$$\rho \frac{\partial^2 v}{\partial t^2} = C_{11} \frac{\partial^2 v}{\partial y^2} \quad .$$

This identifies C_{11}/ρ as the square of the horizontal compressional velocity.

For a z-propagating (u=v=0) compressional wave, the equations become

$$\rho \frac{\partial^2 w}{\partial t^2} = C_{33} \frac{\partial^2 u}{\partial z^2} \quad .$$

This identifies C_{33}/ρ as the square of the vertical compressional velocity.

For shear waves which either propagate in, or are polarized in the z direction, the differential equations reduce to

$$\rho \frac{\partial^2 u}{\partial t^2} = C_{44} \frac{\partial^2 u}{\partial z^2}$$

$$\rho \frac{\partial^2 v}{\partial t^2} = C_{44} \frac{\partial^2 v}{\partial z^2}$$

$$\rho \frac{\partial^2 w}{\partial z^2} = C_{44} \left(\frac{\partial^2 w}{\partial x^2} + \frac{\partial^2 w}{\partial y^2} \right) \quad .$$

This identifies C_{44}/ρ as the square of the shear velocity in the vertical plane.

Shear waves which propagate in, and are polarized in, the plane of bedding obey

$$\rho \frac{\partial^2 u}{\partial t^2} = C_{66} \frac{\partial^2 u}{\partial y^2} \quad ,$$

$$\rho \frac{\partial^2 v}{\partial t^2} = C_{66} \frac{\partial^2 v}{\partial x^2} \quad .$$

This identifies C_{66}/ρ as the square of the shear velocity in the plane of bedding.

In summary, four of the five independent elastic parameters of an anisotropic medium may be associated with compressional and shear velocities in axial directions, as follows:

$$c_{p_z} = (C_{33}/\rho)^{1/2} \quad ,$$

$$c_{p_x} = (C_{11}/\rho)^{1/2} \quad ,$$

$$c_{s_{xy}} = (C_{66}/\rho)^{1/2} \quad ,$$

$$c_{s_z} = (C_{44}/\rho)^{1/2} \quad ,$$

where c_{p_z}, c_{p_x}, $c_{s_{xy}}$, c_{s_z} now denote these velocities. The fifth independent elastic parameter, C_{13}, does not appear directly, and its evaluation requires an off-axial measurement and the use of a dispersion relation. (See Podio et al., 1968.)

C. Plane Wave Solutions to the Equations of Motion

Let us now assume that no quantities in the differential equations are dependent upon y. Under these conditions, the equation for v completely decouples from the equations for u and w, which remain coupled to one another. We complete the reduction to the vertical plane by setting v=0. Subject to these restrictions, the differential equations become

$$\rho \frac{\partial^2 u}{\partial t^2} = C_{11} \frac{\partial^2 u}{\partial x^2} + C_{44} \frac{\partial^2 u}{\partial z^2} + (C_{13}+C_{44}) \frac{\partial^2 w}{\partial z \partial x} \quad ,$$

$$\rho \frac{\partial^2 w}{\partial t^2} = C_{44} \frac{\partial^2 w}{\partial x^2} + C_{33} \frac{\partial^2 w}{\partial z^2} + (C_{13}+C_{44}) \frac{\partial^2 u}{\partial z \partial x} \quad .$$

In the vertical plane, the constant C_{66} does not play a role, as it appears only for motion entirely in the plane of bedding. Therefore, our first important result is that shear anisotropy does not play a role in the problem. The anisotropic properties of our tranversely anisotropic medium affect motion only through the compressional anisotropy and in the behavior of the constant C_{13}.

Let us assume a plane wave form for the displacements,

$$\begin{pmatrix} u \\ w \end{pmatrix} = \begin{pmatrix} u_o \\ w_o \end{pmatrix} \exp(iqz+ik_x x-i\omega t) \quad ,$$

where k_x is the horizontal wave number, assumed from measurements in water, q is the vertical wave number, still to be identified, and ω is the angular frequency.

Substitution of this form into the equations of motion yields

$$-\rho\omega^2 u_o = -C_{11}k_x^2 u_o - C_{44}q^2 u_o - (C_{13}+C_{44})\, k_x q w_o \quad ,$$

$$-\rho\omega^2 w_o = -C_{44}k_x^2 w_o - C_{33}q^2 w_o - (C_{13}+C_{44})\, k_x q u_o \quad .$$

To simplify these equations, define

$$J = C_{13} + C_{44} \quad ,$$

$$T = \rho\omega^2 - C_{11}k_x^2 \quad ,$$

$$S = \rho\omega^2 - C_{44}k_x^2 \quad .$$

These substitutions yield

$$(T-C_{44}q^2)\, u_o - Jqk_x w_o = 0 \quad ,$$

$$(S-C_{33}q^2)\, w_o - Jqk_x u_o = 0 \quad ,$$

which have solution only if

$$\left(T-C_{44}q^2\right)\left(S-C_{33}q^2\right) - J^2k_x^2q^2 = 0 \quad .$$

This consistency equation defines the allowed vertical wave numbers. It is a quadratic in q^2, with solutions

$$q_1^2 = \frac{\Gamma + \sqrt{\Gamma^2 - 4C_{33}C_{44}TS}}{2C_{33}C_{44}}$$

and

$$q_2^2 = \frac{\Gamma - \sqrt{\Gamma^2 - 4C_{33}C_{44}TS}}{2C_{33}C_{44}} \quad ,$$

where

$$r = TC_{33} + SC_{44} + J^2k_x^2 \quad .$$

Thus, the plane wave solution to the equations of motion has two vertical waves allowed and takes the form

$$\begin{pmatrix} u \\ w \end{pmatrix} = \left\{ \begin{pmatrix} u_1 \\ w_1 \end{pmatrix} \exp(iq_1 z) + \begin{pmatrix} u_2 \\ w_2 \end{pmatrix} \exp(iq_2 z) \right\} \exp(ik_x x - i\omega t) \quad .$$

In order to check this solution for the vertical wave number, let us examine the isotropic limit by setting $C_{11}=C_{33}=\lambda+2\mu$, $C_{13}=\lambda$, and $C_{44}=\mu$, where λ and μ are the usual Lamé parameters for isotropic media. The wave numbers for the two allowed plane waves obtained by such a substitution are:

$$q_1^2 = (\rho\omega^2 - \mu k_x^2)/\mu \quad ,$$

$$q_2^2 = (\rho\omega^2 - (\lambda+2\mu))/\mu \quad .$$

Thus the plane wave, in the isotropic case, becomes the familiar purely compressional wave of velocity $((\lambda+2\mu)/\rho)^{1/2}$, and purely shear wave of velocity $(\mu/\rho)^{1/2}$. Thus, q_1 is associated with a quasi-shear wave, while q_2 is associated with a quasi-compressional wave.

This development has already revealed several points of interest. The shear anisotropy does not enter the problem of the propagation of elastic waves in the vertical plane. The coupled wave equations for the displacements differ from the isotropic equations only by having C_{11} and C_{33} where the isotropic equations would have a single constant. This difference is sufficient to prevent a useful separation in potentials; that is, purely shear and compressional waves cannot be defined.

D. Reflection of a Plane Wave from an Anisotropic Solid

Now that the behavior of plane waves in a single infinite medium has been examined, let us proceed to derive the reflection coefficient for plane waves from the fluid side incident upon the boundary between a semi-infinite isotropic ocean and a semi-infinite, transversely anisotropic, solid ocean floor. The coordinate system in which we shall work is standard, the x-y plane being the boundary plane and the positive z-axis extending down into the solid.

The standard boundary conditions apply; that is, vertical displacement, vertical stress, and tangential stress are continuous across the interface. Since the liquid layer cannot support shear waves, the tangential stress must vanish at the interface. The boundary conditions may then be written in the form:

$$-(1-R)ik_o = w_1 + w_2 \quad ,$$

$$(1+R)\rho_o\omega^2 = iC_{33}(q_1w_1+q_2w_2) + iC_{13}k_x(u_1+u_2) \quad ,$$

$$0 = q_1u_1 + q_2u_2 + k_x(w_1+w_2) \quad ,$$

where R is the reflection coefficient, ρ_o is the water density, and k_o is the vertical wave number in the water. These equations correspond, respectively, to continuity of vertical displacement, vertical stress, and horizontal stress. There are five unknowns (R, u_1, u_2, w_1, w_2), and only three boundary equations. The equations of motion provide the remaining two equations needed to solve for the unknowns. Through the relations obtained before we have:

$$0 = \left(T - C_{44}q_1^2\right)u_1 - Jk_x q_1 w_1 \quad ,$$

$$0 = \left(S - C_{33}q_2^2\right)w_2 - Jk_x q_2 u_2 \quad .$$

The system of equations is now soluble, and the reflection coefficient is given by the ratio of determinants:

$$R = \frac{\begin{vmatrix} -ik_o & 1 & 1 & 0 & 0 \\ -i\rho_o\omega^2 & C_{33}q_1 & C_{33}q_2 & C_{13}k_x & C_{13}k_x \\ 0 & k_x & k_x & q_1 & q_2 \\ 0 & -Jk_xq_1 & 0 & T-C_{44}q_1^2 & 0 \\ 0 & 0 & S-C_{33}q_2^2 & 0 & -Jk_xq^2 \end{vmatrix}}{\begin{vmatrix} -ik_o & 1 & 1 & 0 & 0 \\ i\rho_o\omega^2 & C_{33}q_1 & C_{33}q_2 & C_{13}k_x & C_{13}k_x \\ 0 & k_x & k_x & q_1 & q_2 \\ 0 & -Jk_xq_1 & 0 & T-C_{44}q_1^2 & 0 \\ 0 & 0 & S-C_{33}q_2^2 & 0 & -Jk_xq_2 \end{vmatrix}}$$

Upon working the algebra entailed by these determinants, one obtains

$$R = \frac{A - B}{A + B} \quad ,$$

where

$$A = k_o\left[Jk_x^2(q_2-q_1)\left\{C_{33}q_2\left(T-C_{44}q_1^2\right) - C_{13}q_1\left(S-C_{33}q_2^2\right)\right\}\right.$$

$$\left. + \left(C_{33}q_1q_2-C_{13}k_x^2\right)\left\{J^2k_x^2q_1q_2 - \left(S-C_{33}q_2^2\right)\left(T-C_{44}q_1^2\right)\right\}\right] \quad ,$$

and

$$B = \rho_o \omega^2 \left[-q_2 \left(T - C_{44} q_1^2 \right) \left(J k_x^2 + S - C_{33} q_2^2 \right) + J k_x^2 q_2 \left(T + C_{13} q_1 q_2 \right) \right] .$$

On examining the isotropic media limit of this result (making the same substitutions made in the reduction of the wave number), one obtains

$$R = \frac{4k_x^2 q_1 q_2 + \left(k_x^2 - q_1^2 \right)^2 - \left(\frac{\rho_1}{\rho_2} \right) \left(\frac{\omega}{c_s} \right)^4 \left(\frac{q_2}{k_o} \right)}{4k_x^2 q_1 q_2 + \left(k_x - q_1^2 \right)^2 + \left(\frac{\rho_1}{\rho_2} \right) \left(\frac{\omega}{c_s} \right)^4 \left(\frac{q_2}{k_o} \right)} ,$$

which is the usual form for the reflection coefficient found in Ewing, Jardetsky, and Press (1957).

Thus, we have found that we can solve for the reflection coefficient, applying standard matrix techniques to a system of equations containing the standard boundary conditions and two additional equations which our initial demand upon the form of the solution forced from the differential equations. Our solution is somewhat complicated, but reduces in the isotropic limit to a familiar form.

E. Reflection from a Layered Anisotropic Solid

The reflection coefficient having been obtained for two semi-infinite media, the next step is to expand the theoretical framework to include finite layers.

In a finite layer, the displacements now include upward and downward propagating plane waves and take the form

$$w = w_1 \exp(iq_1 z) + w_2 \exp(-iq_1 z)$$

$$+ w_3 \exp(iq_2 z) + w_4 \exp(-iq_2 z) \quad ,$$

$$u = u_1 \exp(iq_1 z) + u_2 \exp(-iq_2 z)$$

$$+ u_3 \exp(iq_2 z) + u_4 \exp(-iq_2 z) \quad ,$$

from which we may obtain the normal stress

$$S_{zz} = i(C_{13}k_x u_1 + C_{33}q_1 w_1) \exp(iq_1 z)$$

$$+ i(C_{13}k_x u_2 - C_{33}q_1 w_2) \exp(-iq_1 z)$$

$$+ i(C_{13}k_x u_3 + C_{33}q_2 w_3) \exp(iq_2 z)$$

$$+ i(C_{13}k_x u_4 - C_{33}q_2 w_4) \exp(-iq_2 z) \quad ,$$

and the tangential stress

$$S_{zx} = i\, C_{44}(k_x w_1 + q_1 u_1) \exp(iq_1 z)$$

$$+ i\, C_{44}(k_x w_2 - q_1 u_2) \exp(-iq_1 z)$$

$$+ i\, C_{44}(k_x w_3 + q_2 u_3)\, \exp(iq_2 z)$$

$$+ i\, C_{44}(k_x w_4 - q_2 u_4)\, \exp(-iq_2 z) \quad .$$

We also have available the relations between the vertical and horizontal displacements which must be satisfied for the existence of a plane wave solution. These relations are similar to those used earlier to solve the problem of two semi-infinite media. They are:

$$0 = \left(T - C_{44} q_1^2\right) u_1 - J q_1 k_x w_1 \quad ,$$

$$0 = \left(T - C_{44} q_1^2\right) u_2 + J q_1 k_x w_2 \quad ,$$

$$0 = \left(S - C_{33} q_2^2\right) u_3 - J q_2 k_x u_3 \quad ,$$

$$0 = \left(S - C_{33} q_2^2\right) u_4 + J q_2 k_x u_4 \quad .$$

These consistency relations can be used to eliminate the horizontal displacements (u_i) in terms of the vertical displacement in the stresses S_{zz} and S_{xz}. This done, we define a vector of quantities which are continuous across an interface between two transversely anisotropic solids.

$$Y = \begin{bmatrix} w \\ S_{zz} \\ S_{zx} \\ u \end{bmatrix}$$

This vector can now be written entirely in terms of the vertical displacements (w_i) by using a matrix format,

$$Y = \begin{bmatrix} 1 & 1 & 1 & 1 \\ i(C_{13}k_xX_1+C_{33}q_1) & -i(C_{13}k_xX_1+C_{33}q_1) & i(C_{13}k_xX_2+C_{33}q_2) & -i(C_{13}k_xX_2+C_{33}q_2) \\ iC_{44}(k_x+X_1q_1) & iC_{44}(k_x+X_1q_1) & iC_{44}(k_x+X_2q_2) & iC_{44}(k_x+X_2q_2) \\ X_1 & -X_1 & X_2 & -X_2 \end{bmatrix}$$

$$\times \begin{bmatrix} G & 0 & 0 & 0 \\ 0 & 1/G & 0 & 0 \\ 0 & 0 & Q & 0 \\ 0 & 0 & 0 & 1/Q \end{bmatrix} \begin{bmatrix} w_1 \\ w_2 \\ w_3 \\ w_4 \end{bmatrix}$$

or Y=E D(z)B, where E is the first matrix, D(z) is the second matrix, and B is the vector containing the vertical displacements. The quantities in the matrices are:

$$G = \exp(iq_1z)$$

$$Q = \exp(iq_2z)$$

$$X_1 = Jq_1k_x/\left(T-C_{44}q_1^2\right)$$

$$X_2 = \left(S-C_{33}q_2^2\right)/Jq_2k_x \quad .$$

The vector Y has two interesting properties. First, it embodies the solutions to the differential equations for plane wave

motion in a transversely anisotropic media. It thus expresses the values of displacement and stress at each point z within a layer. Second, it contains only quantities that are continuous across the interface between two solids.

Using these properties we can now develop the method for computing the reflection coefficient of a plane wave in the ocean incident upon a homogeneously layered, transversely isotropic ocean floor. Let each layer be numbered from 1 to n with the ocean being layer 0 and the semi-infinite substrate being layer n+1. At the top of the layer labeled m, the depth dependent quantities are represented as $Y_m(0)$, and at the bottom of the layer, as $Y_m(H_m)$, where H_m is the thickness of the layer. Thus, the continuity of the stress and displacement across the interface between layers m and m+1 is given by $Y_{m+1}(0)=Y_m(H)$ or

$$E_{m+1}\ B_{m+1} = E_m D(H_m) B_m \quad .$$

This can be rewritten as

$$B_{m+1} = E_{m+1}^{-1}\ E_m D(H_m) B_m \quad ,$$

where E_{m+1}^{-1} is the inverse of the matrix E_{m+1}.

In the substrate layer, the fact that no further reflections occur reduces the displacements to downward propagating plane waves only:

$$W = A_1 \exp(iq_1 z) + A_2 \exp(iq_2 z)$$

$$U = A_3 \exp(iq_1 z) + A_4 \exp(iq_2 z) \quad .$$

The consistency relations which allow plane wave solutions are

$$\left(T-C_{44}q_q^2\right)A_1 - Jk_xq_1A_3 \quad ,$$

$$\left(S-C_{33}q_2^2\right)A_2 - Jk_xq_2A_4 \quad ,$$

yielding, upon substitution into the definition of stress, the vector

$$Y_{n+1} = A_1\begin{bmatrix} 1 \\ (C_{33}q_1+C_{13}k_xX_1) \\ iC_{44}(k_x+q_1X_1) \\ X_1 \end{bmatrix} + A_2\begin{bmatrix} 1 \\ (C_{33}q_2+C_{13}k_xX_2) \\ iC_{44}(k_x+q_2X_2) \\ X_2 \end{bmatrix}$$

or

$$Y_{n+1} = A_1N + A_2L \quad ,$$

where N and L are the first and second vectors, respectively, in the equation for Y_{n+1} above, and

$$X_1 = \left(T-C_{44}q_1^2\right)/Jk_xq_1 \quad ,$$

$$X_2 = \left(S-C_{33}q_2^2\right)/Jk_xq_2 \quad .$$

Therefore, in terms of the amplitudes at the top of the first solid layer, the substrate stresses and displacements are

$$Y_{n+1} = A_1 N + A_2 L = \left[\prod_{m=1}^{1} (E_m D_m (H_m) E_m^{-1}) \right] Y_1(0) \quad ,$$

$$= PB_1 \quad ,$$

where P is the product matrix through which the unknown amplitudes in the intermediate layers are eliminated.

In the top semi-infinite fluid layer, however, we have

$$Y_o = \begin{bmatrix} -ik_o(1-R) \\ \rho_o \omega^2 (1+R) \\ 0 \\ 0 \end{bmatrix} = Y_o^o + Y_o^1 R \quad ,$$

where

$$Y_o^o = \begin{bmatrix} -ik_o \\ \rho_o \omega^2 \\ 0 \\ 0 \end{bmatrix}$$

and

$$Y_o^1 = \begin{bmatrix} ik_o \\ \rho_o\omega^2 \\ 0 \\ 0 \end{bmatrix} \quad .$$

Since the fluid does not support tangential displacements, the transition of the first interface is handled by writing

$$Y_1(0) = Y_o + \begin{bmatrix} 0 \\ 0 \\ 0 \\ u_o \end{bmatrix} \quad ,$$

where u_o is the unconstrained horizontal displacement at the top of the first layer. Substituting for $Y_1(0)$ in the equation for Y_{n+1} yields the system of linear equations which must be solved to obtain the reflection coefficient

$$A_1N + A_2L - PY_o^1R - P_{\cdot 4}u_o = PY_o^o \quad ,$$

where $P_{\cdot 4}$ is the fourth column of the matrix P. As there are only four unknown quantities in this relation (A_1, A_2, R, u_o), a solution may be obtained via any number of standard methods for linear equations.

Thus, we have established a method by which the reflection coefficient can be obtained for a system containing an arbitrary number

of layers in which the unknown displacement amplitude of intermediate layers do not appear. This method differs from that for isotropic layers in that equations relating to displacement amplitude obtained from the differential equations must be used to reduce the matrices to a form in which the movement from one layer to another can be handled by a simple multiplication of matrices. The evaluation of the formal solution is obviously a matter for the computer.

CHAPTER IV

PROPERTIES OF THE REFLECTION COEFFICIENTS

In our computation of reflection coefficients we have utilized a standard environment. The semi-infinite layer in which the plane waves originate is water, with a sound speed of 1550 m/sec and a density of 1.043 g/cm^3. The underlying solid layers have elastic parameters which are discussed below. Our computations have been made at a standard frequency of 50 Hz.

The primary difficulty in obtaining meaningful results from the theory developed above lies in the paucity of published data on values for the elastic parameters. We have located, to date, only three full sets of elastic parameters. The earliest were obtained from Podio et al. (1968), and are recapitulated in Tables II and III. These two samples correspond, respectively, to compressional anisotropies (computed according to the formula in Chapter II) of 2.81% and 3.89%. The latest set of parameters were obtained by Jones and Wang (1981) for cretaceous shales from the Williston Basin, and are recapitulated in Table IV. This set of parameters corresponds to a compressional anisotropy of 20.6%. Thus, while our samples are few, nevertheless realms of both high and of low anisotropy are represented.

In Section IV.A, we discuss the effects sediment anisotropy has on the vertical wave number, and note the possibility of backward

TABLE II

ANISOTROPIC ELASTIC PARAMETERS FOR GREEN RIVER SHALE,

MEASURED UNDER 8000 psi CONFINING PRESSURE*

Shale Density 2.35 g/cm^3

Parameter	Value (kbars)	Velocity (m/sec)
C_{11}	476	4500
C_{33}	450	4243
C_{44}	154	2556
C_{13}	170	2690

*Data from Podio et al. (1968)

TABLE III

ANISOTROPIC ELASTIC PARAMETERS FOR GREEN RIVER SHALE,

MEASURED UNDER 1000 psi CONFINING PRESSURE*

Shale Density 2.35 g/cm^3

Parameter	Value (kbars)	Velocity (m/sec)
C_{11}	441	4332
C_{33}	408	4167
C_{44}	132	2370
C_{13}	143	2467

*Data from Podio et al. (1968)

TABLE IV

ANISOTROPIC ELASTIC PARAMETERS FOR

WILLISTON BASIN CRETACEOUS SHALE*

Shale Density 2.42 g/cm^3

Parameter	Value (kbars)	Velocity (m/sec)
C_{11}	343	3765
C_{33}	227	3063
C_{44}	54	1494
C_{13}	107	2103

*Data from Jones and Wang (1981)

traveling phase fronts. Section IV.B deals with the effects of anisotropy on reflection from hard sediments. In Section IV.C a scheme to approximate the constant C_{13} is considered, and in Section IV.D, the effects of anisotropy on reflection from soft sediments is examined.

A. Effects of Anisotropy on Wave Numbers

Since the vertical wave numbers q_1 and q_2 only reduce to their normal form in the limit of isotropy, it is of interest to observe their behavior for the transversely anisotropic media before proceeding to the computation of the surface reflection coefficient.

Plots in the complex plane of q_1 and q_2 for Green River Shale under 8000 psi confining pressure are contained in Fig. 1. In this figure, solid lines represent regions of overlays of q_1 and q_2, dotted lines represent q_1 only, and dashed lines represent q_2 only; the grazing angles are marked for reference. Recall that q_1 is the quasi-shear vertical wave number and q^2 is the quasi-compressional vertical wave number, based on their behavior in the isotropic limit. Figure 1 shows that, as in the isotropic case, each wave number has a purely real part corresponding to transmission into the sediment and a purely imaginary part corresponding to total reflection from the sediment. The total reflection occurs due to velocities in sediment being greater than that in water. The anisotropic case also has a region at very low grazing angle (in this case up to 10°) in which the vertical wave numbers are neither purely real nor purely imaginary. This region does not occur for isotropic media. In this range q_2 is approximately equal to $-q_1^*$.

The existence of negative values for the real part of the vertical wave number q_1 indicates that in this range there are backward

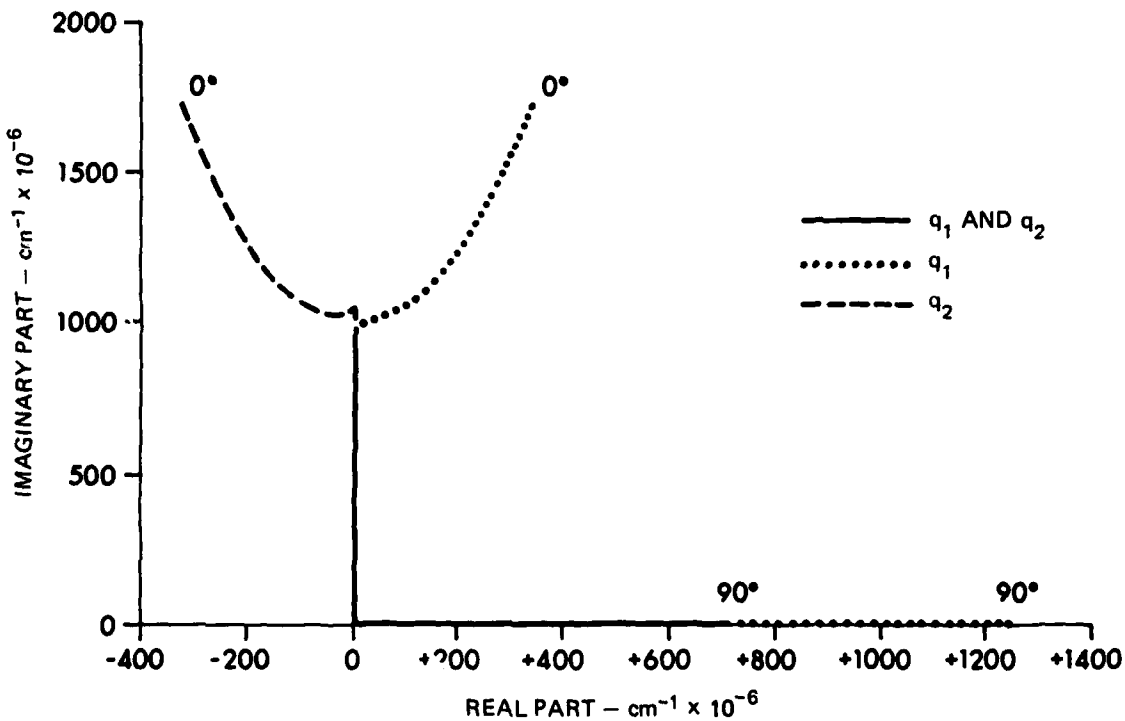

FIGURE 1
THE VERTICAL WAVE NUMBERS IN THE COMPLEX PLANE

ARL:UT
AS-82-684
DWO-GA
5-10-82

traveling phase fronts, i.e., phase fronts traveling toward the interface from the solid side. As will be discussed below, this quirk of the vertical wave number does not affect the reflection coefficient.

The off-axis complex vertical wave numbers occurred for input data in which the velocity contrast between media was very high. For Green River shale at 1000 psi confining pressure, the region in which the vertical wave numbers are neither purely real nor purely imaginary becomes much shorter, and for Williston Basin shale, which has no zone of total reflection, it vanishes altogether. Thus, such a phenomenon would most likely occur in an oceanic environment of exposed basalts or hard sediments rather than in the normal gradual layering from ooze to hard sediments to basalt.

Two important results appear from this study of the vertical wave number. First, in hard sediments we may see, at low grazing angles, wave numbers which represent propagating but heavily damped waves. Second, waves of this type, which corresponds to a quasi-shear wave, will be propagated backwards, towards the interface.

B. Effects of Anisotropy on Fluid-Solid Interface Reflection Coefficient

In computing the surface reflection coefficient R, we will find that measured anisotropies produce observable changes in both the magnitude and phase of R when compared to the isotropic case. We will compute bottom loss curves for such surfaces, where $BL = -20 \log_{10} |R|$. The sediments studied here are those for which full sets of anisotropic parameters have been measured, i.e., the shales described in Tables II-IV. These materials do not correspond to the soft, unconsolidated

material found over much of the ocean floor, but are more typical of exposed basalt and outcropping sedimentary rocks.

In Figs. 2-7, we compare computations of bottom loss and the phase of the reflection coefficient for isotropic and anisotropic consolidated sediments. On each figure solid curves represent isotropic computations, and dashed curves represent anisotropic curves. Figures 2 and 3 show bottom loss and phase of the reflection coefficient, respectively, for a Green River shale under 8000 psi confining pressure; Figs. 4 and 5 show these quantities for a Green River shale under 1000 psi confining pressure; and Figs. 6 and 7 show the same for a Williston Basin shale.

For the high velocity Green River shales (see Figs. 2-5), the realm of total reflection (below 53° for the shale of Figs. 2 and 3 and below 49° for that of Figs. 4 and 5) remains unchanged by the addition of anisotropy. The greatest change in bottom loss, Figs. 2 and 4, occurs in the range of angle intermediate between the critical angles associated with the two wave numbers. The critical angles are defined as the angles at which the associated vertical wave numbers change from being purely imaginary to being purely real, i.e., the angle above which the wave propagates into the solid. That angle associated with the quasi-shear wave number q_1 is the first (smallest) critical angle, and the angle associated with the quasi-compressional wave number q_2 is the second (larger) critical angle. Between the two wave numbers, anisotropic bottom loss differs from isotropic bottom loss by about 0.2 dB, and a prominent (1 dB) lowering of bottom loss occurs at the second critical angle (about 70°), probably due to a sampling error related to

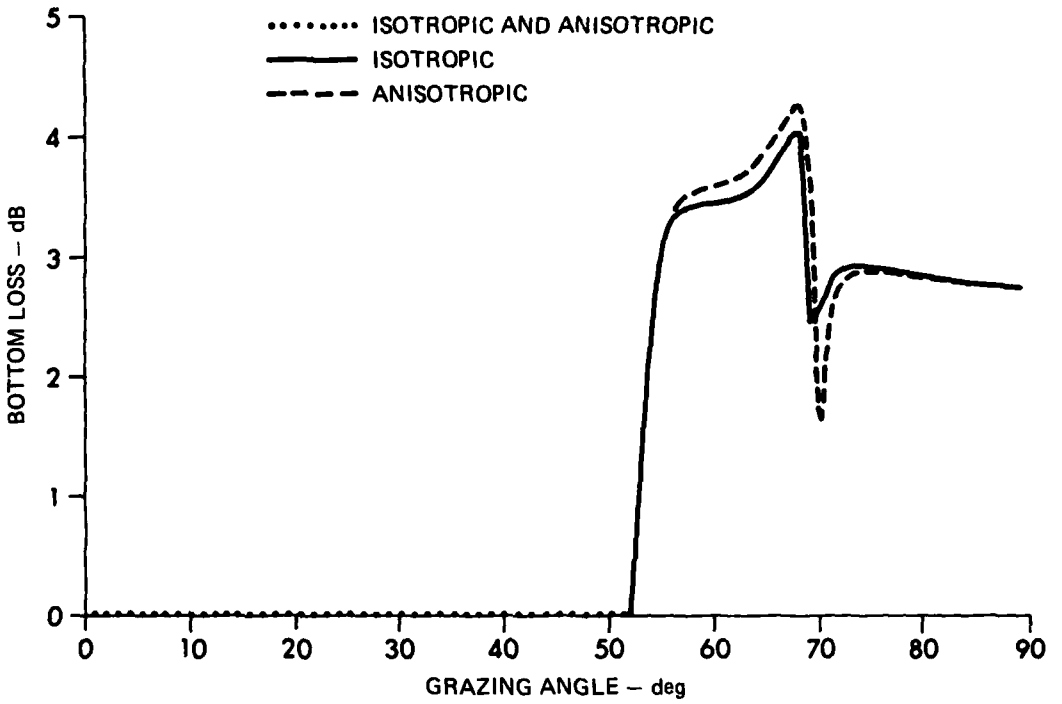

FIGURE 2
BOTTOM LOSS FOR FAST GREEN RIVER SHALE

ARL:UT
AS-82-685
DWO - GA
5 - 10 - 82

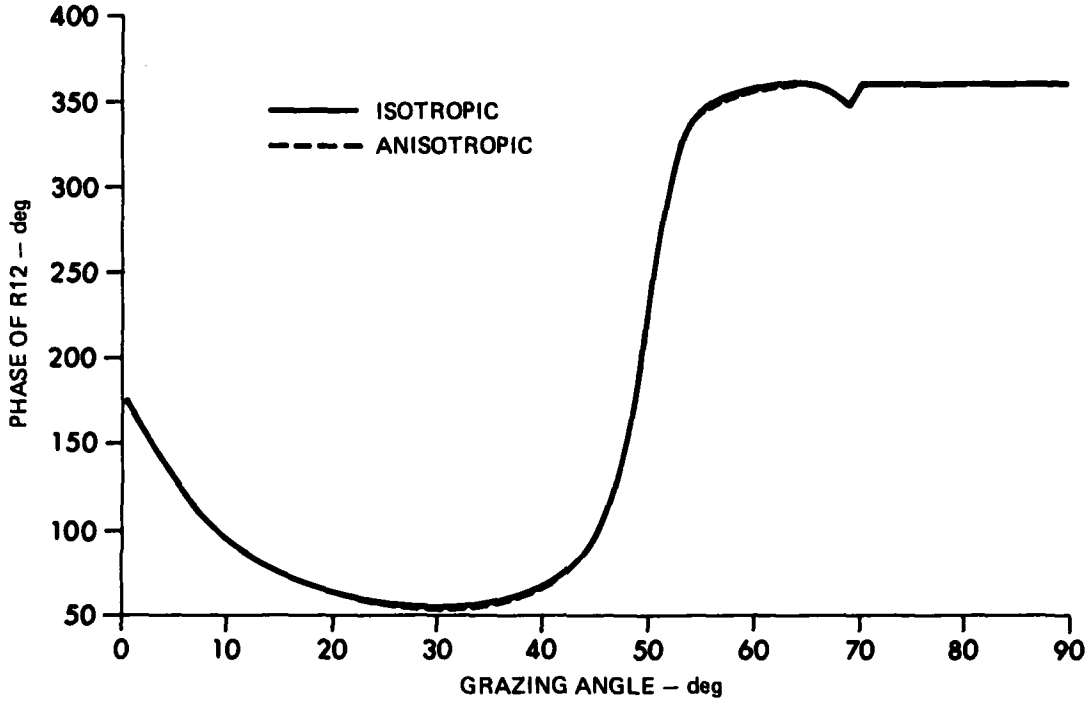

FIGURE 3
PHASE OF REFLECTION COEFFICIENT FOR FAST GREEN RIVER SHALE

ARL:UT
AS-82-686
DWO - GA
5 - 10 - 82

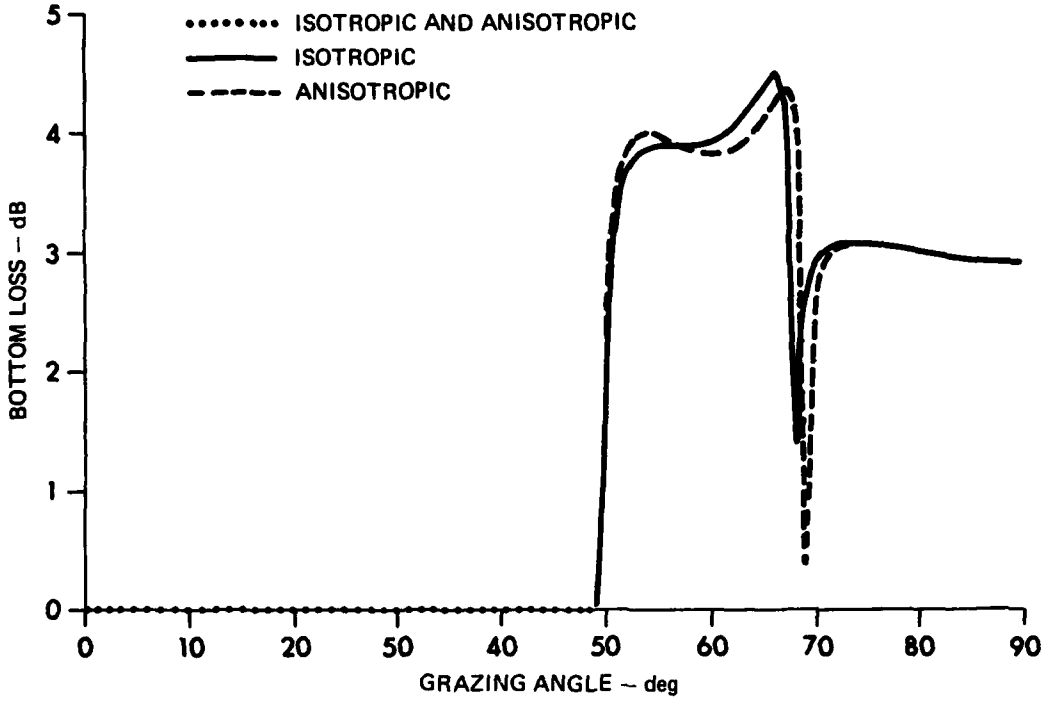

FIGURE 4
BOTTOM LOSS FOR SLOW GREEN RIVER SHALE

ARL:UT
AS-82-687
DWO - GA
5 - 10 - 82

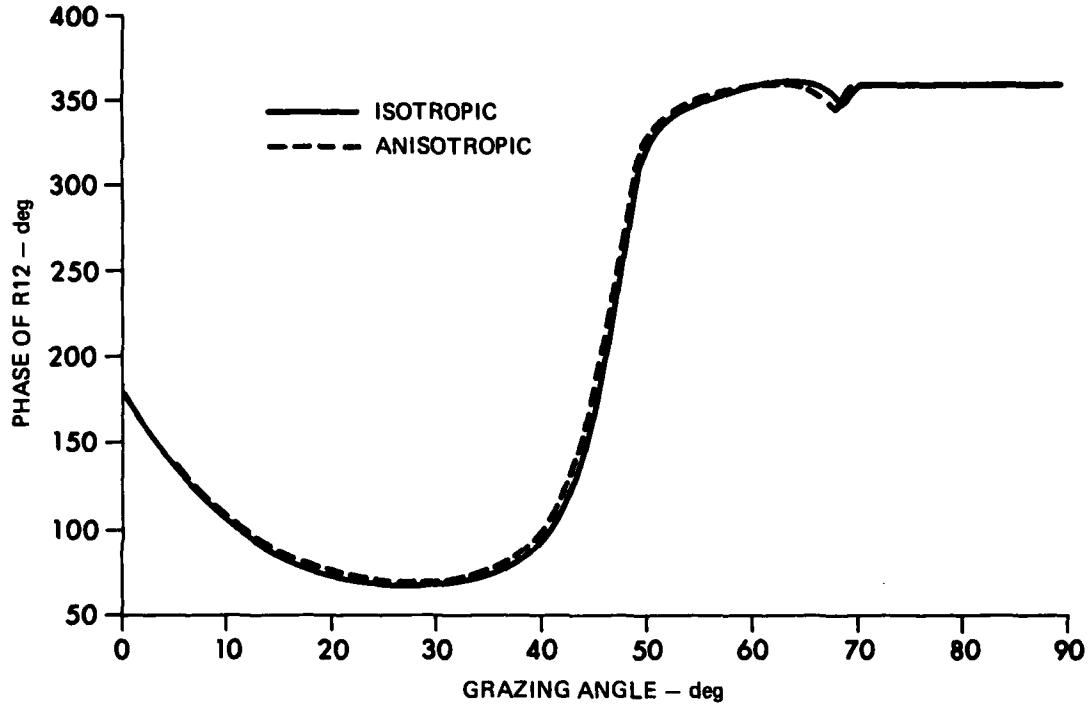

FIGURE 5
PHASE OF REFLECTION COEFFICIENT FOR SLOW GREEN RIVER SHALE

ARL:UT
AS-82-688
DWO - GA
5 - 10 - 82

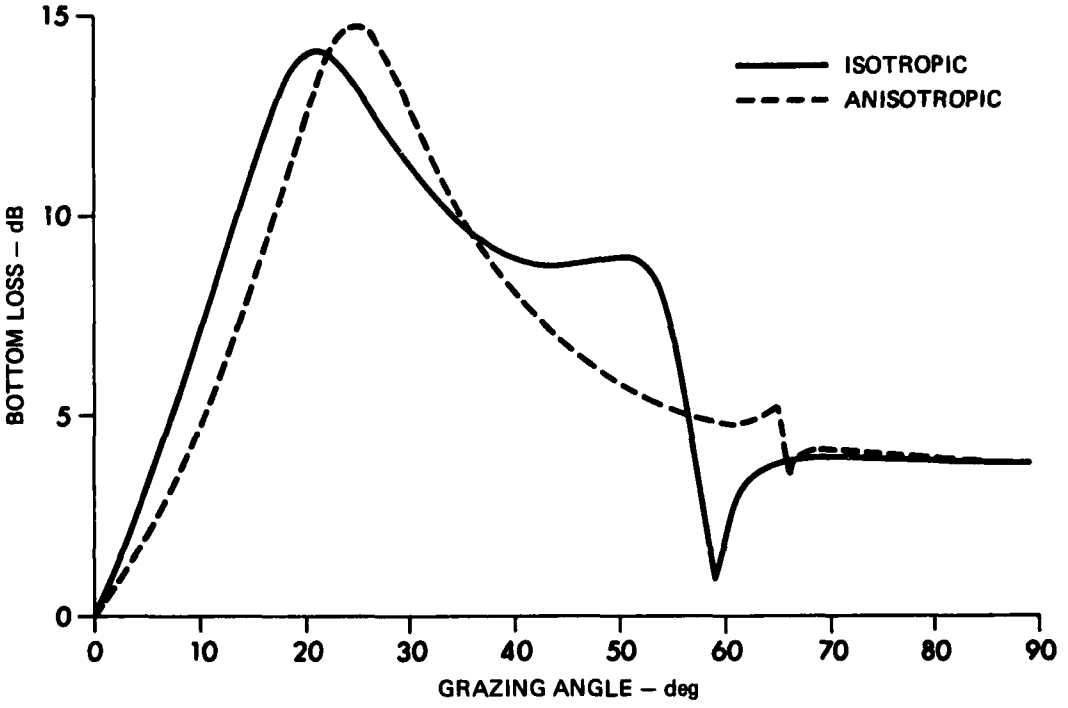

FIGURE 6
BOTTOM LOSS FOR WILLISTON BASIN SHALE

ARL:UT
AS-82-689
DWO - GA
5 - 10 - 82

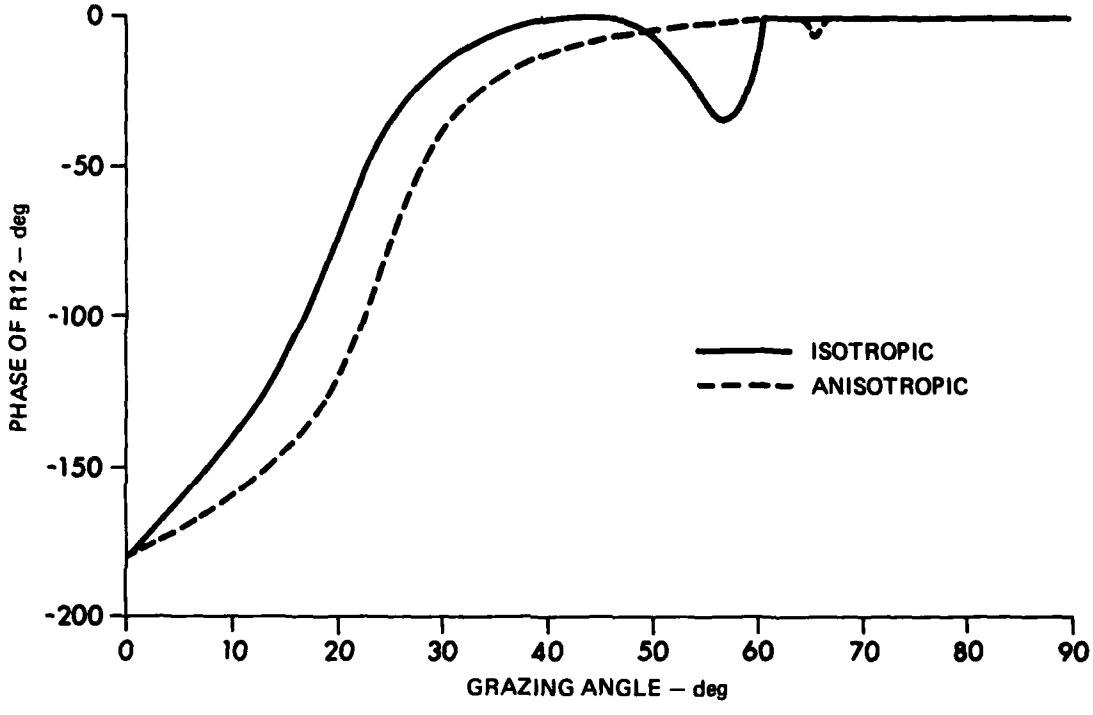

FIGURE 7
PHASE OF REFLECTION COEFFICIENT FOR WILLISTON BASIN SHALE

ARL:UT
AS-82-690
DWO - GA
5 - 10 - 82

1° increments used in computation. Furthermore, note that the location of this critical angle is shifted by almost 2°

The change in the phase of the reflection coefficient is about 2° for the first of these shales (Fig. 3), and 7° for the second shale (Fig. 5) near the second critical angles, becoming much less away from these angles.

For the Williston Basin shale (Fig. 6), however, there is no range of total reflection since the shear velocity is smaller than the water sound speed. The anisotropy changes bottom loss for this case at angles from zero to second critical angle (67°). Of most interest, however, is a marked decrease in bottom loss of about 2 dB at low grazing angles. The shift in the second critical angle is much more pronounced here, approximately 8°.

Drastic effects are to be seen in the phase for the Williston Basin shale (Fig. 7). The phase of the reflection coefficient for the anisotropic shale differs from that for the isotropic shale by as much as 120° below a grazing angle of 67°. The two become practically indistinguishable above this grazing angle.

In this section we have shown that transverse anisotropy yields nontrivial differences in bottom loss and the phase of the reflection coefficient when compared to the same quantities in isotropic sediments. The curves are not qualitatively different, and most of the effects seem attributable to the distortion in the curves due to a shift in the position of the critical angle for quasi-compressional waves. The differences in bottom loss amount to as little as a few tenths of decibels for low anisotropy sediments (Green River shale), to as much as 3.5 dB

for a moderately high anisotropy sediment (Williston shale). Phase differences range from 2° for low anisotropy sediments to as much as 120° for high anisotropy sediments.

C. Parameter Studies on the Constant C_{13}

One problem in our analysis has been a lack of measurements of the constant C_{13}. The determination of C_{13} requires the use of the dispersion relation or consistency equation for the differential equation, and a measurement of the speed of one of the wave solutions to the differential equations in some specified non-axial direction. This non-axial measurement is not normally made. Furthermore, a certain modicum of error in C_{13} is bound to result in its computation from the dispersion relation, the components of which are experimentally determined.

Until measurements become readily available, it is of interest to consider how good an approximation might be made of the actual value of this elastic parameter. In this section we develop a means for estimating C_{13} for consolidated (hard) sediments for which the compressional wave anisotropy is measured.

A parameterization of the constant C_{13} must have two properties. It must reduce to the isotropic value in some simple limit, and it must be simpler in form than the dispersion relation.

In this isotropic limit C_{13} reduces to λ, i.e.,

$$C_{13} = C_{33} - 2C_{44} = \left(c_{p_z}^2 - 2c_s^2\right)\rho \quad .$$

Let us parameterize C_{13} as

$$C_{13} = \beta \sqrt{C_{11}C_{33}} - 2C_{44} \quad .$$

This reduces to the isotropic limit when β=1 and C_{11}=C_{33}. The parameter β is then defined by the relation

$$\beta = \frac{C_{13} + 2C_{44}}{\sqrt{C_{11}C_{33}}} \quad .$$

If we divide out density from the defining equation for β, and express the result in terms of shear and compressional velocities, we obtain the relation

$$\beta \approx \frac{(\alpha + \alpha_1)}{\alpha_2} \left(\frac{c_s}{c_p}\right)^2 \quad ,$$

where α_1 is of order unity and relates C_{13} to C_{44}, while α_2 is the constant of proportionality relating C_{11} to C_{33}.

Experimentally obtained values for C_{13} (Tables II-IV) show that C_{13} is of the order of C_{44} for mildly anisotropic sediments or is some small multiple of C_{44} for strongly isotropic sediments, i.e., α_1 is of magnitude one or two. The Williston Basin shale has C_{13} approximately equal to twice C_{44}. Likewise, the term $\sqrt{C_{11}C_{33}}$ will always be greater than C_{33} for transverse isotropy. A measured anisotropy, of 100%, computed according to the definitions of Chapter II, would yield

$$\sqrt{C_{11}C_{33}} = 3C_{33} \quad .$$

Therefore, we safely consider that $1<\alpha_2<3$. Thus, the values of α_1 and α_2, which are the values most likely to occur in marine sediments, and the fact that $c_s<c_p$ demand that $\beta<1$.

Let us then vary β from its actual computed values for the sediments available to us until we reach $\beta=1$, in order to determine precisely to what extent inaccuracy in β affects the reflection coefficients. Fortunately, in all cases, the greatest effect of variation of β occurs in the vicinity of the second critical angle. For the Green River shales the bottom loss curves (see Figs. 8 and 9) are undisturbed below the quasi-shear critical angles. Near the quasi-compressional critical angle ($\sim$70°), the bottom loss curves are gradually displaced to a maximum of about 0.3 dB (in Fig. 8).

Beyond the quasi-shear critical angles, phases of the reflection coefficient show displacements for these low anisotropy shales similar to those they encounter in a total reduction to isotropy; about 1° for the lowest anisotropy shale and about 5° for the higher anisotropy shale. We omit graphs of these phases, as the curves so overlay one another as to be indistinguishable.

In the case of the Green River shale, where there is no region of total reflection, bottom loss at the lower grazing angle is affected less than 0.1 dB (see Fig. 10), even though phenomena near the critical angle for quasi-compressional waves are displaced by approximately 0.5 dB in the full reduction to $\beta=1$. However, the region of lower grazing angles where greatest effect of anisotropy occurred is not

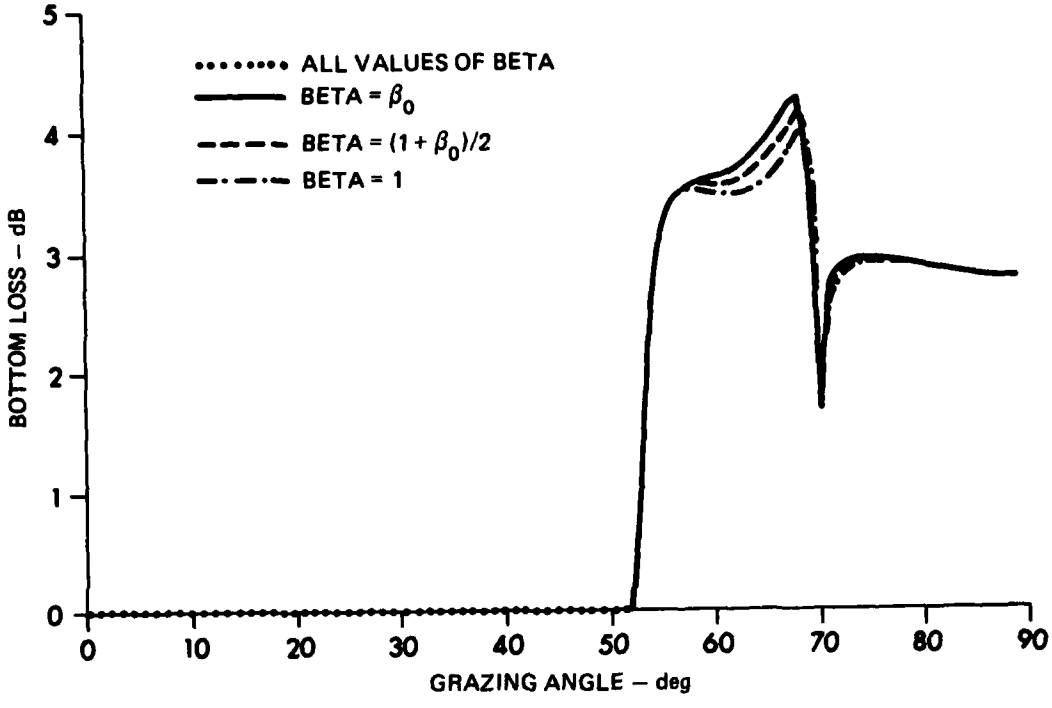

FIGURE 8
GRADUAL REDUCTION OF BETA TO 1; EFFECTS ON BOTTOM LOSS FOR FAST GREEN RIVER SHALE

ARL:UT
AS-82-691
DWO - GA
5 - 10 - 82

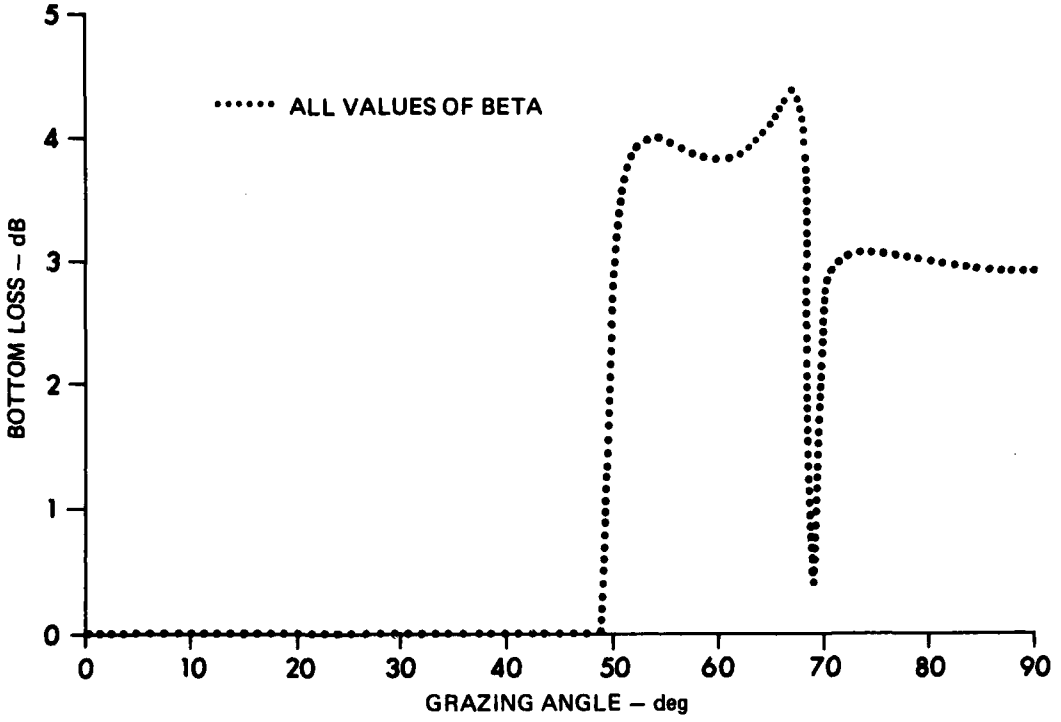

FIGURE 9
GRADUAL REDUCTION OF BETA TO 1; EFFECTS ON BOTTOM LOSS FOR SLOW GREEN RIVER SHALE

ARL:UT
AS-82-692
DWO - GA
5 - 10 - 82

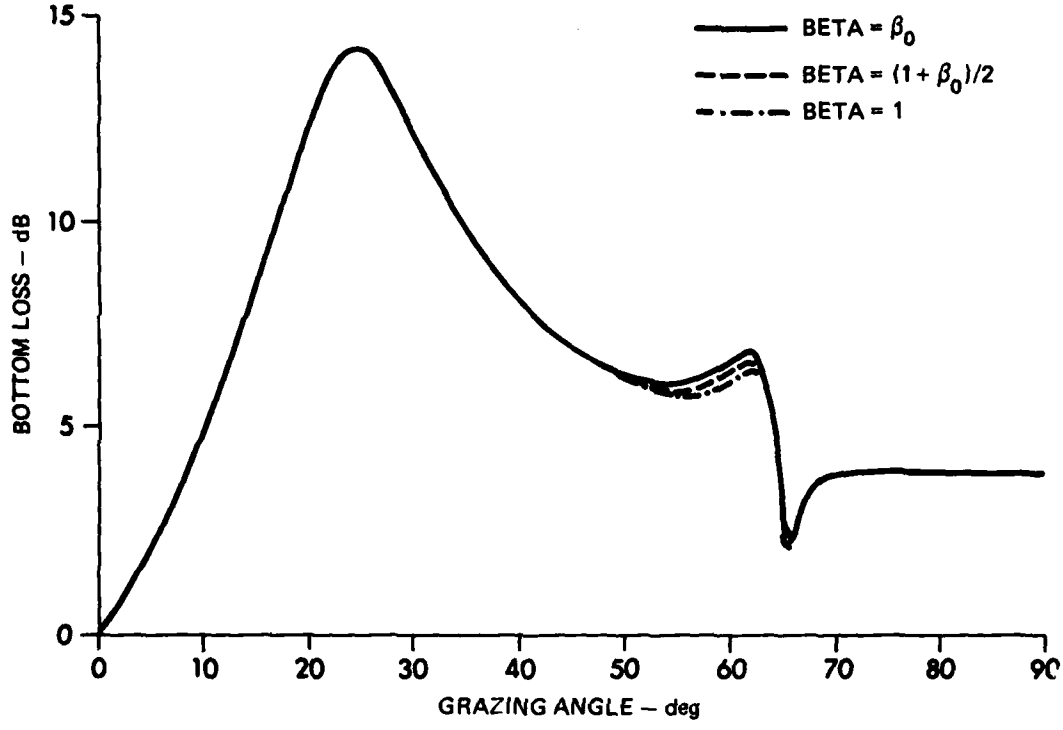

FIGURE 10
GRADUAL REDUCTION OF BETA TO 1; EFFECTS ON BOTTOM LOSS FOR WILLISTON BASIN SHALE

ARL:UT
AS-82-693
DWO - GA
5 - 10 - 82

changed as β is varied. The phases of the reflection coefficient for this shale also show very little disturbance as β is reduced to one (Fig. 11). The total disturbance in phase over the whole range of angles is 5° in the worst case.

Thus we have seen that variations in the parameter β lead to small scale variations in bottom loss in the region of the critical angle for quasi-compressional waves. Changes in the phase of the reflection coefficient are also small. Thus we may safely make the approximation $\beta=1$, for consolidated sediments. For hard sediments, therefore, no great loss in precision occurs in using the approximation

$$C_{13} = \sqrt{C_{11}C_{33}} - 2C_{44} \quad .$$

D. Effects of Anisotropy on Reflection from a Typical Marine Sediment

The preceding sections dealt with hard sediments in which the densities and the compressional and shear velocities were high. In typical near-surface silt-clay sediment, the compressional velocity will be lower than that of the water, and the shear velocity will be of an order of magnitude less than the compressional velocity. It is of interest to determine whether bottom loss curves for soft sediments are affected in the same manner that they are for hard sediments.

If we use a water velocity of 1550 m/sec and a water density of 1.043 g/cm^3, we may use the ratio of sediment compressional velocity to water compressional velocity of 0.98 given in Bachman (1979) to obtain a sediment compressional velocity of 1520 m/sec. Use of the velocity

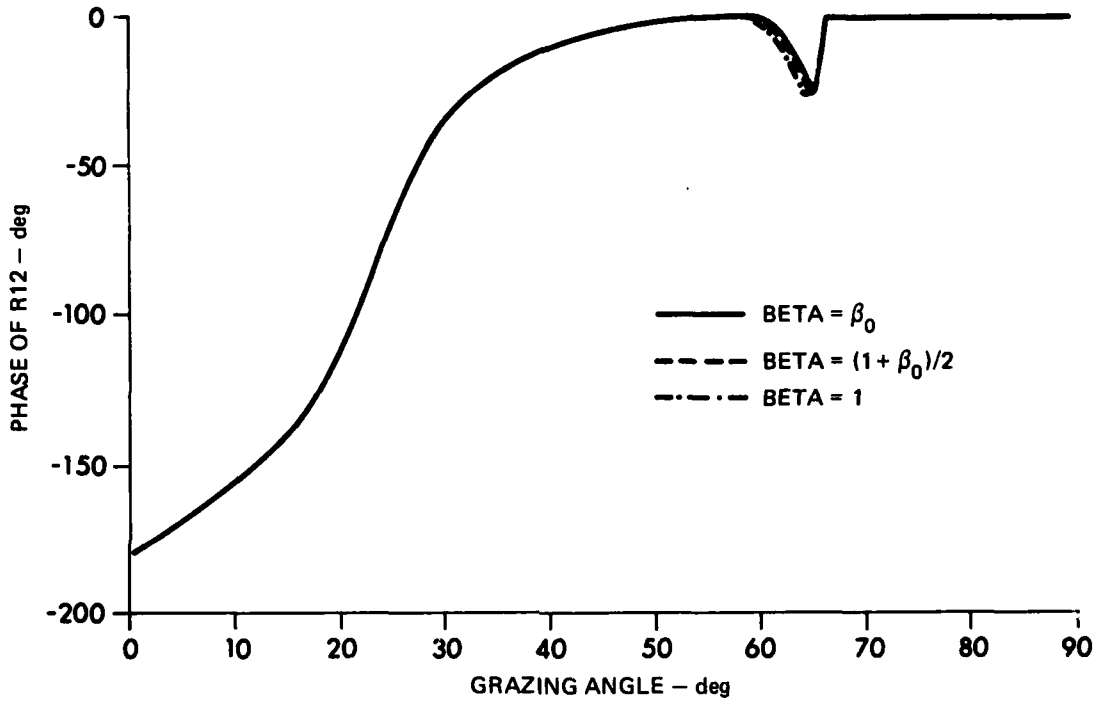

FIGURE 11
GRADUAL REDUCTION OF BETA TO 1; EFFECTS ON PHASE OF REFLECTION COEFFICIENT FOR WILLISTON BASIN SHALE

ARL:UT
AS-82-694
DWO - GA
5 - 10 - 82

density curve given in Hamilton (1978) yields a sediment density of 1.65 g/cm^3. We use a shear velocity of 115 m/sec (Hamilton, 1976).

At this point a difficulty in interpretation arises. Is the sediment compressional velocity obtained from this ratio a vertical velocity, a horizontal velocity, or some sort of mean velocity? Since Bachman provides no answer to this question, we will compute bottom loss curves for each of the three possibilities: $c_p=\sqrt{c_{p_z} c_{p_x}}$, $c_p=c_{p_z}$, and $c_p=c_{p_x}$. The precise distribution of velocity between horizontal and vertical is obtained via the regression formula of Bachman (1979) for silt-clays, $V_v = 0.25 + 0.83\ V_h$, where V represents compressional velocity in units of km/sec and subscripts v and h denote vertical and horizontal directions, respectively. Bottom loss for the isotropic case is computed as a reference. A summary of these four distributions of velocity is contained in Table V.

With this information we can compute the elastic parameters:

$$C_{11} = c_{p_x}^2 \rho \quad ,$$

$$C_{33} = c_{p_z}^2 \rho \quad ,$$

$$C_{44} = c_s^2 \rho \quad ,$$

where ρ is the density, c_{p_x} is the horizontal compressional velocity, c_{p_z} is the vertical compressional velocity, and c_s is the shear velocity. However, this is not enough information to compute the parameter C_{13}.

TABLE V

POSSIBLE INTERPRETATIONS OF CALCULATED COMPRESSIONAL VELOCITY

FOR ANISOTROPIC AND ISOTROPIC SEDIMENTS

	c_p (m/sec)	c_{p_x} (m/sec)	c_{p_z} (m/sec)
Mean $c_p=\sqrt{c_{p_x} c_{p_z}}$	1520	1525	1515
Vertical $c_p=c_{p_z}$	1520	1530	1520
Horizontal $c_p = c_{p_x}$	1520	1520	1512
Isotropic	1520	1520	1520

Let us therefore utilize the parameterization of C_{13} obtained in Section IV.C, and set

$$C_{13} = \beta \sqrt{C_{11}C_{13}} - 2C_{44} \quad .$$

For hard sediments it was determined that we could safely set β=1. This proves nothing for soft sediments, however, since the magnitude of β for soft sediments is not known. Therefore, bottom loss curves will be computed at various values of β to determine the effect of anisotropy and the sensitivity to β.

In Fig. 12 we see bottom loss computed at β=1 for the four distributions of velocity outlined in Table V. The principal effect of the transverse anisotropy has been an increase in bottom loss near the angle of intromission where the peak in bottom loss occurs. The actual value of bottom loss at the angle of intromission is not significant due to increments used in computation. The various assignments of the values of compressional velocities lead to a scatter over about 3° of the location of the angle of intromission. The assignment $c_p=c_{p_x}$ leads to an angle of intromission identical with that for the isotropic case. The other assignments, $c_p=\sqrt{c_{p_z}c_{p_x}}$ and $c_p=c_{p_z}$, lead to shifts in the position of angle of intromission of 2° and 3°, respectively.

In Fig. 13 we see bottom loss computed at β=0.75 for the four distributions of velocity outlined in Table V. The cluster of values of the angle of intromission has displaced about 6° from the angle of intromission for an isotropic sediment. This displacement of the angle of intromission has so displaced the curve that in the range of grazing angle

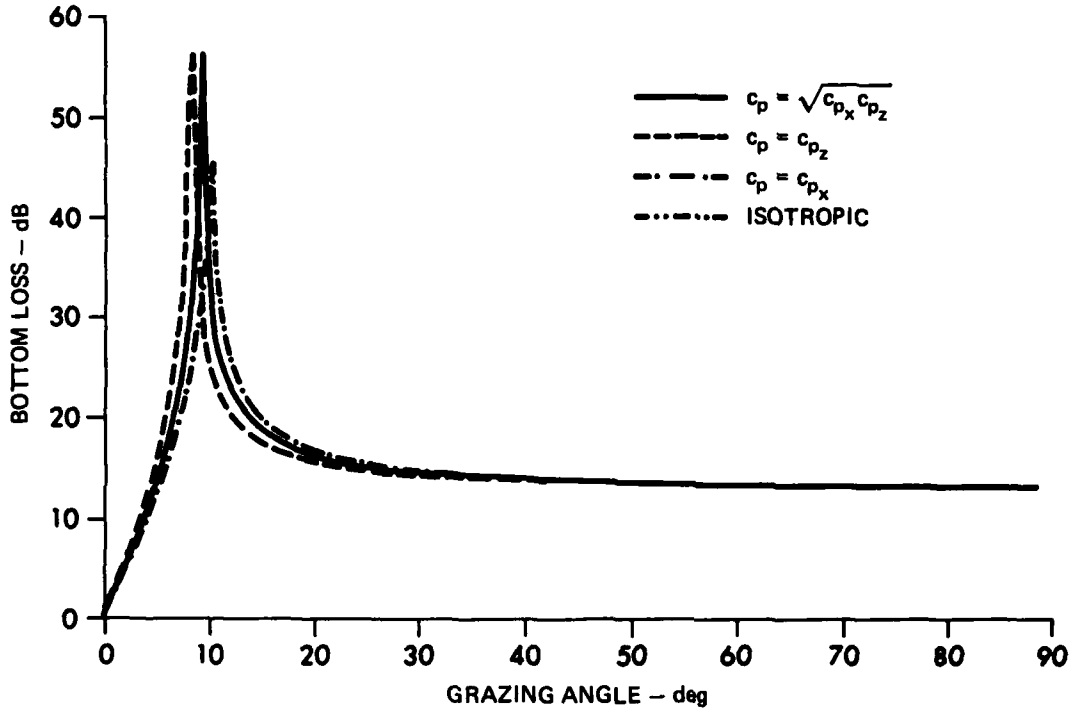

FIGURE 12
BOTTOM LOSS FROM SOFT SILT-CLAY SEDIMENT; BETA = 1

ARL:UT
AS-82-695
DWO - GA
5 - 10 - 82

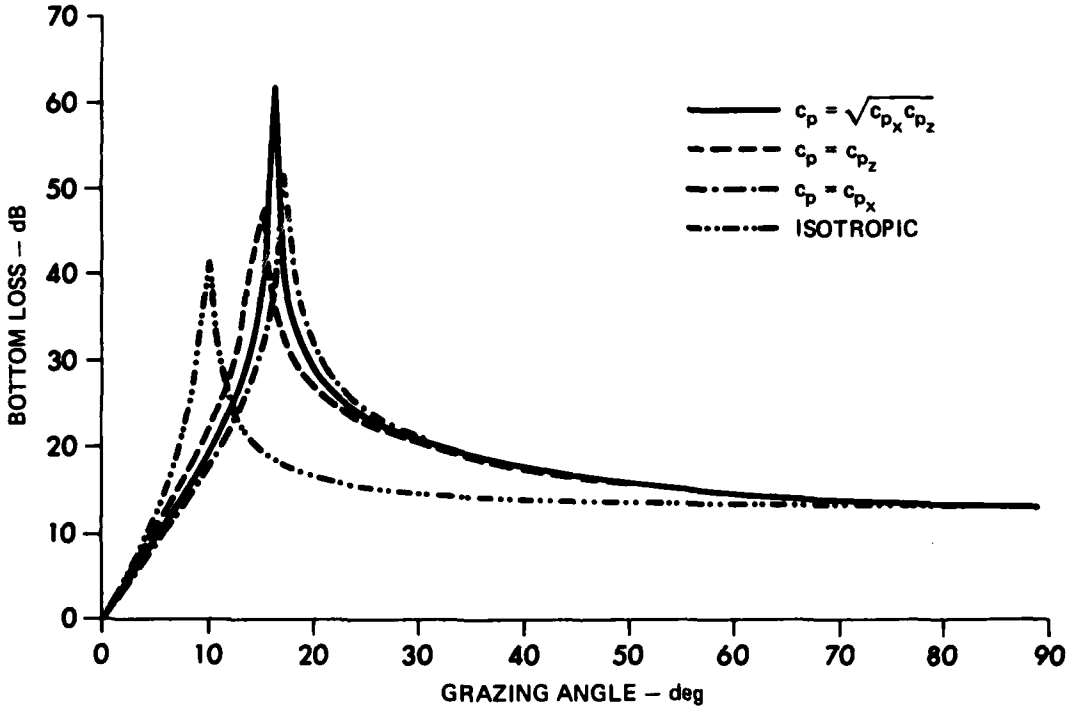

FIGURE 13
BOTTOM LOSS FROM SOFT SILT-CLAY SEDIMENT; BETA = 0.75

ARL:UT
AS-82-696
DWO - GA
5 - 10 - 82

from 5° to 70° the difference in bottom loss varies over the range from 1 dB (at the endpoints of the range of grazing angle) to 55 dB at the new angle of intromission, and is of the order of 10 dB over large reaches of grazing angle.

In Fig. 14, the bottom loss has been computed at β=0.5 for the four distributions of velocity outlined in Table V. The angle of intromission has shifted even further, now approximately 25° beyond that for an isotropic sediment, and differences in bottom loss similar to those discussed in the preceding paragraph are now spread over the range of grazing angles from 0° to 80°.

At this point enough of a trend has been established to assert that the location of the angle of intromission is very sensitive to the value of the parameter β. If, however, this parameter is of the order obtained for hard sediments, i.e., somewhere between 0.7 and 1.0, and closer to 1.0 for less anisotropic sediments, the approximation β=1 obtained in Section IV.C should hold. The final verdict on this point must obviously await the actual measurement of the elastic parameter C_{13} for soft sediments.

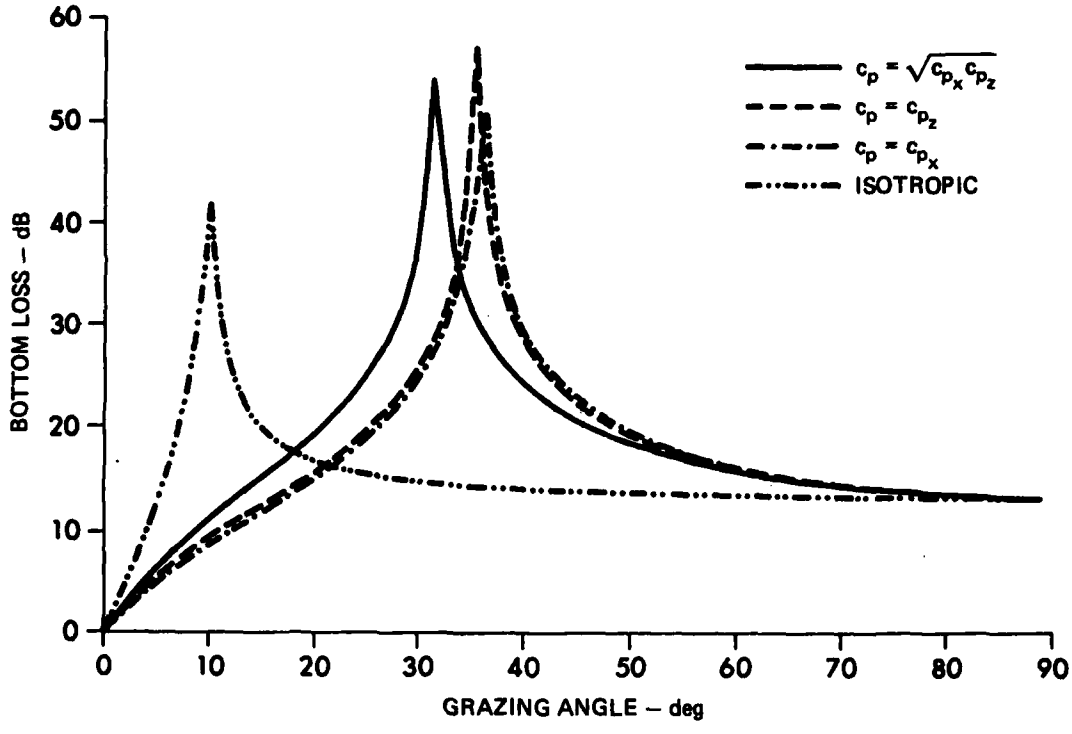

FIGURE 14
BOTTOM LOSS FROM SOFT SILT-CLAY SEDIMENT; BETA = 0.5

ARL:UT
AS-82-697
DWO - GA
5 - 10 - 82

CHAPTER V

CONCLUSIONS

Previous mathematical formulations of the problem of reflection from the sea floor have assumed that the sea floor is an isotropic solid. It was always known, however, that this was at best an approximation. Recent geological studies, summarized above, have led to the view that the sea floor can be better modeled as a transversely isotropic solid.

The equations of motion for transversely isotropic media depend on five elastic parameters rather than two. For motion in only the vertical plane, one of these elastic parameters has no effect. The elimination of this one parameter, however, also eliminates consideration of shear anisotropy, as only a single shear velocity occurs in the equations of motion for the vertical plane. Shear anisotropy is important only for motion entirely within a horizontal plane.

The assumption of plane wave solutions to the equations of motion yields an equation of consistency leading to two solutions for the vertical wave number. One corresponds to quasi-compressional motion, and the other to quasi-shear motion. An examination of the vertical wave number shows that it is possible, in environments of velocity contrast sufficient to have realms of total reflection, to have backward traveling phase fronts.

Using standard boundary conditions, we solve for the reflection coefficient between two semi-infinite media, and set up the system of equations for layered media in a form amenable to computer solution. We show that the reflection coefficient does reduce, in the isotropic limit, to the usual form.

Studies of reflection from consolidated anisotropic sediments using available sets of parameters were presented. These show that velocity anisotropy alters bottom loss significantly, particularly in sediments for which the velocity contrast is such that the region of total reflection vanishes, or is greatly curtailed. The degree of bottom loss change from isotropy appears to be an increasing function of anisotropy, and even for fairly moderate anisotropies is large enough to measure. In highly anisotropic consolidated sediments, the deviation from isotropic bottom loss amounts to 1 dB over a wide range of low grazing angles, and in all cases the position of the critical angle for compressional waves is shifted more than 1°.

The principal bar to calculating meaningful results on the effect of anisotropy lies in the fact that few full sets of elastic parameters have been measured. We have shown, however, that this deficiency can be obviated for consolidated sediments by using measured compressional wave anisotropy to approximate the elastic parameter C_{13} (which is rarely measured). The approximation is especially good if low grazing angle phenomena are of greater concern than those of high grazing angle.

For soft (unconsolidated) sediments we have estimated full sets of elastic parameters and calculated bottom loss. If, as in the case of

hard sediments, a low anisotropy sediment corresponds to a value of the parameter C_{13} very close to its value in the isotropic limit, the approximation discussed above is valid for soft sediments, and the principal effect of anisotropy in soft (silt-clay) sediments is a small shift (1-3°) in the angle of intromission. If this is not true, we have shown that bottom loss is very sensitive to the value of β. Obviously, more information is needed on the actual value of the constant C_{13} in soft sediments.

In the work completed so far, we have shown that compressional anisotropy has significant effects on both bottom loss and the phase of the reflection coefficient for both consolidated and unconsolidated sediments. The course of future work in this topic seems obvious. The assumption of isovelocity layers must be abandoned and standard linear gradients in velocity adopted. This would include refraction phenomena known to be important in isotropic media. The computational tools already stand in such form that the effect of anisotropy on energy absorption can be taken into account. Additional work may also be done on a topic totally excluded from this paper, that of surface (interface) waves.

BIBLIOGRAPHY

Aki, Keiiti, and Paul G. Richards, Quantitative Seismology (W. H. Freeman and Co., San Francisco, 1980).

Anderson, Don L., "Elastic Wave Propagation in Layered Anisotropic Media," J. Geophys. Res. 66, 2953-2963 (1961).

Bachman, Richard T., "Acoustic Anisotropy in Marine Sediments and Sedimentary," J. Geophys. Res. 84, 7661-7663 (1979).

Backus, George E., "Long-Wave Elastic Anisotropy produced by Horizontal Layering," J. Geophys. Res. 67, 4427-4440 (1962).

Bain, G. W., "Geological Chemical and Physical Problems in the Marble Industry," Tech. Publ. 1261, American Institute of Mining and Metallurgical Engineering, New York, 1940.

Bukry, D., "Cenozoic Calcareous Nannofossils from the Pacific Ocean," Trans. San Diego Soc. Nat. Hist. 16, 303 (1971).

Carlson, R. L., and N. I. Christensen, "Velocity Anisotropy in Semi-Indurated Calcareous Deep-Sea Sediments," J. Geophys. Res. 84, 205-211 (1979).

Dandekar, D. P., "Elastic Constants of Calcite," J. Appl. Phys. 39, 2971-2973 (1968).

Ewing, W. Maurice, Wencelas S. Jardetzky, and Frank Press, Elastic Waves in Layered Media (McGraw-Hill Book Company, Inc., New York, 1957).

Hamilton, Edwin, "Sound Velocity and Related Properties of Marine Sediments, North Pacific," J. Geophys. Res. 75, 4423-4446 (1970).

Hamilton, Edwin, "Shear Velocity versus Depth in Marine Sediments: A Review," Geophysics 41, 985-996 (1976).

Hamilton, Edwin, "Velocity versus Density in Sediments and Rocks," J. Acoust. Soc. Am. 63, No. 2, 366-377 (1978).

Jones, Leonie E. A., and Herbert Wang, "Ultrasonic Velocities in Cretaceous Shales from the Williston Basin," Geophysics 46, 288-297 (1981).

LeRoy, L. W., Subsurface Geologic Methods, 2nd ed. (Colorado School of Mines, Golden, Colorado, 1950).

Love, A. E. H., Treatise on the Mathematical Theory of Elasticity, 4th ed. (Dover Publications, New York, 1944).

Manghnani, M. H., S. O. Schlanger, and P. D. Milholland "Elastic Properties Related to Depth of Burial, Strontium Content and Age, and Diagenetic State in Pelagic Carbonate Sediments," in Bottom Interacting Ocean Acoustics, edited by William A. Kuperman and Finn B. Jensen (Plenum Press, New York, 1980).

Milholland, P. D., M. H. Manghnani, S. O. Schlanger, and G. H. Sutton, "Geoacoustic Modeling of Deep-Sea Carbonate Sediments," J. Acoust. Soc. Am. 68, 1351 (1980).

Podio, A. L., A. R. Gregory, K. E. Gray, "Dynamic Properties of Dry and Water-Saturated Green River Shale under Stress," Soc. Petr. Eng. 8, 389-404 (1968).

Schlanger, S. O., and R. G. Douglas, "Pelagic Ooze-Chalk-Limestone Transition and Its Implications for Marine Stratigraphy, Pelagic Sediments: On Land and Under the Sea," Spec. Publ. 1, International Association of Sedimentology, London, 1974, p. 117.

Stoneley, Robert, "The Seismological Implication of Aeolotropy in Continental Structure, Monthly Notices Roy. Astron. Soc. Geophys. Suppl. 5, 343-353 (1949).

Uhrig, L. F., and F. A. Van Melle, "Velocity Anisotropy in Stratified Media," Geophysics 20, 774 (1955).

Weyl, P. K., "Pressure Solution and the Force of Crystalization - A Phenomenological Theory," J. Geophys. Res. 64, No. 11, 2001 (1952)..

1 June 1982

DISTRIBUTION LIST FOR
ARL-TR-82-28
UNDER CONTRACT N00014-80-C-0490
UNCLASSIFIED

Copy No.	
1	Commanding Officer Office of Naval Research Arlington, VA 22217 Attn: Robert D. Ryan (Code 400R)
	Commanding Officer Naval Ocean Research and Development Activity NSTL Station, MS 39529
2	Attn: W. A. Kuperman (Code 320)
3	CDR M. McCallister (Code 520)
4	J. Matthews (Code 360)
5	G. Morris (Code 340)
6	W. W. Worsley (Code 530)
	Commanding Officer Office of Naval Research Arlington, VA 22217
7	Attn: P. Rogers (Code 425AC)
8	Office of Naval Research Branch Office, Chicago Department of the Navy 536 South Clark Street Chicago, IL 60605
	Commanding Officer Naval Electronic Systems Command Washington, D.C. 20360
9	Attn: LCDR S. Hollis (Code 612)
	Director Naval Research Laboratory Department of the Navy Washington, D.C. 20375
10	Attn: B. B. Adams (Code 8160)
11	W. Mosley

Copy No.

Commanding Officer
Naval Ocean Systems Center
Department of the Navy
San Diego, CA 92152
12 Attn: E. L. Hamilton
13 M. A. Pederson
14 H. P. Bucker

Commander
Naval Sea Systems Command
Department of the Navy
Washington, D.C. 20362
15 Attn: R. W. Farwell (Code 63RA)

Chief of Naval Material
Department of the Navy
Washington, D.C. 20360
16 Attn: CAPT E. Young (Code MAT 08T245)

17 Commander
Naval Surface Weapons Center
White Oak Laboratory
Department of the Navy
Silver Spring, MD 20910

18 Commander
David W. Taylor Naval Ship Research and
Development Center
Department of the Navy
Bethesda, MD 20034

Naval Oceanographic Office
Department of the Navy
NSTL Station, MS 39529
19 Attn: W. Jobst (Code 3400)
20 M. G. Lewis (Code 7200)

Commander
Naval Air Development Center
Department of the Navy
Warminister, PA 18974
21 Attn: C. L. Bartberger

Officer in Charge
New London Laboratory
Naval Underwater Systems Center
Department of the Navy
New London, CT 06320
22 Attn: B. Cole

Superintendent
Naval Postgraduate School
Monterey, CA 93940
23 Attn: Library

Commander
Naval Coastal Systems Center
Department of the Navy
Panama City, FL 32407
24 Attn: G. McLeroy

25 - 36 Commanding Officer and Director
Defense Information Service Center
Cameron Station, Building 5
5010 Duke Street
Alexandria, VA 22314

Woods Hole Oceanographic Institution
86-95 Water Street
Woods Hole, MA 02543
37 Attn: R. Spindel

Science Applications, Inc.
1710 Goodridge Drive
McLean, VA 22101
38 Attn: J. Hanna

Applied Research Laboratory
The Pennsylvania State University
P. O. Box 30
State College, PA 16801
39 Attn: S. McDaniel

Department of Physics
The University of Auckland
Private Bag
Auckland, New Zealand
40 Attn: Alick C. Kibblewhite

Distribution List for ARL-TR-82-28 under Contract N00014-80-C-0490 (Cont'd)

Copy No.

Marine Physical Laboratory of
The Scripps Institution of Oceanography
The University of California, San Diego
San Diego, CA 92132
41 Attn: F. Fisher
42 G. Shor

Scripps Institution of Oceanography
The University of California, San Diego
La Jolla, CA 92037
43 Attn: Library

Bell Telephone Laboratories, Inc.
Whippany Road
Whippany, NJ 07961
44 Attn: S. A. Kramer

Planning Systems, Inc.
7900 Westpark Drive, Suite 507
McLean, VA 22101
45 Attn: R. Cavanaugh

Defence Scientific Establishment
HMNZ Dockyard
Devonport, Auckland
NEW ZEALAND
46 Attn: K. M. Guthrie

School of Mechanical Engineering
Georgia Institute of Technology
Atlanta, GA 30332
47 Attn: A. D. Pierce

Department of Geology and Geophysics
Geophysical and Polar Research Center
Lewis G. Weeks Hall for Geological Sciences
The University of Wisconsin, Madison
1215 W. Dayton Street
Madison, WI 53706
48 Attn: C. S. Clay

Courant Institute
251 Mercer Street
New York, NY 10012
49 Attn: D. C. Stickler

Copy No.

Bolt, Beranek, & Newman, Inc.
50 Moulton Street
Cambridge, MA 02138
50 Attn: H. Cox

Hawaii Institute of Geophysics
The University of Hawaii
2525 Correa Road
Honolulu, HI 96822
51 Attn: G. Sutton
52 L. N. Frazer

Director
North Atlantic Treaty Organization
SACLANT ASW Research Centre
APO New York 09019
53 Attn: T. Akal

Defence Research Establishment Pacific
CF Dockyard
Victoria, BC
CANADA
54 Attn: Ross Chapman

Defence Research Establishment Atlantic
9 Grove Street
P. O. Box 1012
Dartmouth, NS
CANADA
55 Attn: D. Chapman

Rosenteil School of Marine and
Atmospheric Science
The University of Miami
10 Rickenbacker Causeway
Miami, FL 33149
56 Attn: H. DeFarrari

Applied Physics Laboratory
The Johns Hopkins University
Johns Hopkins Road
Laurel, MD 20810
57 Attn: J. Lombardo

Distribution List for ARL-TR-82-28 under Contract N00014-80-C-0490 (Cont'd)

Copy No.

The University of Miami
10 Rickenbacker Causeway
Miami, FL 33149
58 Attn: F. Tappert

Department of Physics
The University of Rhode Island
Kingston, RI 02881
59 Attn: C. Kaufman

Department of Electrical Engineering
Polytechnic Institute of New York
Farmingdale, NY 11735
60 Attn: L. B. Felsen

61 I. Tolstoy
Knockvennie, Castle Douglas
S. W. SCOTLAND
GREAT BRITAIN

Department of Geology
The University of Texas at Austin
Austin, TX 78712
62 Attn: C. Wilson

Department of Physics
The University of Auckland
Private Bag, Auckland
NEW ZEALAND
63 Attn: C. T. Tindle

Brown University
Providence, RI 02912
64 Attn: A. O. Williams, Jr.

The Lamont-Doherty Geological Observatory
Columbia University
Palisades, NY 10964
65 Attn: R. D. Stoll

66 Office of Naval Research
Resident Representative
Room No. 582, Federal Building
Austin, TX 78701

67 Environmental Sciences Division, ARL:UT

Distribution List for ARL-TR-82-28 under Contract N00014-80-C-0490 (Cont'd)

Copy No.	
68	Terry L. Foreman, ARL:UT
69	Robert F. Gragg, ARL:UT
70	Robert A. Koch, ARL:UT
71	Stephen K. Mitchell, ARL:UT
72	Paul J. Vidmar, ARL:UT
73	Reuben H. Wallace, ARL:UT
74	Library, ARL:UT
75 - 85	Reserve, ARL:UT